

Intestinal Bacterial Translocation Contributes to Diabetic Kidney Disease

Hoang Thuy Linh ,¹ Yasunori Iwata,^{1,2} Yasuko Senda,² Yukiko Sakai-Takemori,² Yusuke Nakade,² Megumi Oshima ,¹ Shiori Nakagawa-Yoneda,¹ Hisayuki Ogura,¹ Koichi Sato,¹ Taichiro Minami,¹ Shinji Kitajima,^{1,3} Tadashi Toyama,¹ Yuta Yamamura ,¹ Taro Miyagawa ,¹ Akinori Hara,¹ Miho Shimizu ,¹ Kengo Furuichi,⁴ Norihiko Sakai,^{1,3} Hiroyuki Yamada,⁵ Katsuhiko Asanuma,⁵ Kouji Matsushima,⁶ and Takashi Wada¹

Due to the number of contributing authors, the affiliations are listed at the end of this article.

ABSTRACT

Background In recent years, many studies have focused on the intestinal environment to elucidate pathogenesis of various diseases, including kidney diseases. Impairment of the intestinal barrier function, the “leaky gut,” reportedly contributes to pathologic processes in some disorders. Mitochondrial antiviral signaling protein (MAVS), a component of innate immunity, maintains intestinal integrity. The effects of disrupted intestinal homeostasis associated with MAVS signaling in diabetic kidney disease remains unclear.

Methods To evaluate the contribution of intestinal barrier impairment to kidney injury under diabetic conditions, we induced diabetic kidney disease in wild-type and MAVS knockout mice through unilateral nephrectomy and streptozotocin treatment. We then assessed effects on the kidney, intestinal injuries, and bacterial translocation.

Results MAVS knockout diabetic mice showed more severe glomerular and tubular injuries compared with wild-type diabetic mice. Owing to impaired intestinal integrity, the presence of intestine-derived *Klebsiella oxytoca* and elevated IL-17 were detected in the circulation and kidneys of diabetic mice, especially in diabetic MAVS knockout mice. Stimulation of tubular epithelial cells with *K. oxytoca* activated MAVS pathways and the phosphorylation of Stat3 and ERK1/2, leading to the production of kidney injury molecule-1 (KIM-1). Nevertheless, MAVS inhibition induced inflammation in the intestinal epithelial cells and KIM-1 production in tubular epithelial cells under *K. oxytoca* supernatant or IL-17 stimulation. Treatment with neutralizing anti-IL-17 antibody treatment had renoprotective effects. In contrast, LPS administration accelerated kidney injury in the murine diabetic kidney disease model.

Conclusions Impaired MAVS signaling both in the kidney and intestine contributes to the disrupted homeostasis, leading to diabetic kidney disease progression. Controlling intestinal homeostasis may offer a novel therapeutic approach for this condition.

JASN 33: 1105–1119, 2022. doi: <https://doi.org/10.1681/ASN.2021060843>

Diabetic kidney disease (DKD) is a major complication of diabetes mellitus. DKD increases not only the incidence of ESKD but also the mortality rate in patients with diabetes.¹ Therefore, understanding disease pathogenesis is a particularly important challenge toward innovating novel therapeutic interventions.

Currently, accumulating studies have focused on the intestinal environment to elucidate pathogenesis in various diseases.^{2,3} For kidney diseases,

Received June 22, 2021. Accepted February 22, 2022.

Published online ahead of print. Publication date available at www.jasn.org.

See related editorial, “Of mice and MAVS-diabetic kidney disease and the leaky gut” on pages 1053–1055.

Correspondence: Dr. Yasunori Iwata, Department of Nephrology and Laboratory Medicine, Kanazawa University, 13-1 Takara-machi, Kanazawa 920-8641, Japan. Email: iwatay@staff.kanazawa-u.ac.jp

Copyright © 2022 by the American Society of Nephrology

the gut microbiota plays a role through metabolites.^{4–7} Gut-associated lymphoid tissues (GALTs) are major sites of host encounter with exogenous antigens and pathogens, and the interaction of GALTs with the microbiota regulates both the quality and quantity of systemic immune responses.⁸ The intestinal microbiome plays a major part in the maintenance of immune homeostasis and may affect immune responses at distant sites.^{9–11} A cross-sectional pilot study revealed qualitative differences in the profile of the circulatory microbiome, with lower diversity and significant variations in patients with CKD compared with healthy controls.¹² Moreover, hyperglycemia is reportedly associated with alterations in the epithelial barrier of the gut.¹³ The impairment of the intestinal barrier function, referred to as the “leaky gut,” contributes to pathologic processes in some diseases.^{14–16} These findings prompted us to explore whether intestinal disorders may play a significant role in the development of DKD through the translocation of microbial compounds.

Mitochondrial antiviral signaling protein (MAVS; also known as CARDIF, VISA, and IPS-1) is an adaptor of the retinoic acid-inducible gene (RIG)-I-like receptors (RLRs) such as RIG-I and melanoma differentiation-associated protein (MDA)-5 that plays a central role in the antiviral innate immune.^{17,18} The RLR/MAVS pathway has been implicated in the detection of intracellular bacteria.^{19,20} Mounting evidence indicates that MAVS signaling contributes to regulating intestinal permeability. MAVS deficiency leads to changes in the gut bacterial composition and increased intestinal permeability during some diseases. Then, bacterial translocation within the lymphoid organs leads to increased cytokine production and disease severity.^{21–23}

Therefore, we performed nephrectomy and multiple low-dose streptozotocin (STZ) treatments in wild-type (WT) and MAVS knockout (KO) mice to evaluate the contribution of intestinal barrier impairment to kidney injury under diabetic conditions.

METHODS

Mice

WT C57BL/6J mice were obtained from Charles River Laboratories (Atsugi, Japan). MAVS KO mice generated on a C57BL/6 background were purchased from Jackson Laboratory. All mice were housed and bred at Kanazawa University. All animal experiments were performed following the guidelines of Kanazawa University for animal care and were approved by the Institute for Experimental Animals, Kanazawa University Advanced Science Research Center (registration number, AP-194072).

Diabetic Model

Male mice were nephrectomized at 6–7 weeks of age. Mice were anesthetized *via* intraperitoneal (i.p.) injection with

Significance Statement

Intestinal barrier dysfunction—a “leaky gut”—reportedly contributes to pathological processes in some diseases. In a mouse model, the authors induced diabetic kidney disease, leading to impaired intestinal integrity and inflammation, with IL-17 upregulation. This allowed intestine-derived *Klebsiella oxytoca* and elevated IL-17 to translocate to the circulation and kidneys, then accelerate kidney injury, especially in diabetic knockout mice lacking mitochondrial antiviral signaling protein (MAVS). Stimulation of tubular epithelial cells with *K. oxytoca* activated the MAVS pathway and phosphorylation of Stat3 and ERK1/2, leading to production of kidney injury molecule-1 (KIM-1). Systemic MAVS is renoprotective in diabetic mice by an intestinal protective role and the dominant inhibitory effects on suppressing KIM-1 expression under *K. oxytoca* supernatant or IL-17 stimulation. Controlling intestinal homeostasis may offer a therapeutic strategy in diabetic kidney disease.

0.75 mg/kg body wt medetomidine (Domitor; Orion Corporation), 4 mg/kg midazolam (Sandoz), and 5 mg/kg butorphanol (Vetorphale; Meiji Seika Pharma). Atipamezole (0.75 mg/kg body wt Antisedan; Orion Corporation) was used to reverse the sedative and analgesic effects after the operation was completed. After 2 weeks, the mice were given i.p. injections of 50 mg/kg STZ (Sigma-Aldrich) dissolved in 0.1 M sodium citrate buffer (pH 4.5) for 5 consecutive days. The blood glucose level was measured after 2 weeks using the glucometer system StatStrip Xpress (Nova Biomedical). Mice were considered patients with diabetes when their blood glucose levels were ≥ 300 mg/dl after two consecutive determinations randomly. Mice were monitored for body weight, blood pressure, blood glucose, and collected urine monthly. Sham mice (sex- and age-matched) were nephrectomized and received only sodium citrate buffer i.p. for 5 consecutive days.

Albumin and creatinine levels were measured as detailed in Supplemental Materials and Methods.

Renal Histopathology

The kidneys were fixed in 4% neutral-buffered formalin (Nacalai) and embedded in paraffin. The paraffin blocks were cut into 2- μ m sections and stained with periodic acid-Schiff. The slides were analyzed using the ImageJ software.²⁴

Immunostaining and Immunoblotting

Tissue and cultured cell samples were prepared for immunostaining and Western blot as previously described^{13,25–27} and detailed in Supplemental Materials and Methods.

Intestinal Permeability Assay with FITC-Dextran 4 kDa

On the day of the assay, 4-kDa FITC-dextran (Sigma-Aldrich) was dissolved in PBS to a concentration of 60 mg/ml. Mice were food and water fasted for 4 hours before gavage with 60 mg/100-g body wt FITC-dextran. Three hours after administration, the mice were euthanized to collect their

serum, urine, and kidneys, as described in detail in Supplemental Materials and Methods.

ELISA

IL-17 concentration in the blood was determined using the mouse IL-17 IQELISA Kit (RayBiotech). Urinary neutrophil gelatinase-associated lipocalin (NGAL) levels were measured using the Mouse Lipocalin-2/NGAL Quantikine ELISA Kit (MLCN20, R&D Systems), according to the manufacturer's instructions.

Assessment of Bacterial Translocation

Bacteria-targeted 16S in paraffin-embedded kidney sections was assessed by FUJIFILM Wako using a fluorescence *in situ* hybridization (FISH) assay. Blood, spleen, kidney, and mesenteric lymph nodes were aseptically collected and processed for bacterial culture. Further details are given in Supplemental Materials and Methods.

LPS Administration

When hyperglycemia was well established, 4 weeks after initial STZ administration, WT diabetic mice were anesthetized and laparotomized (1-cm incision). A filled mini-pump was introduced into the peritoneal cavity, and the muscle layer was sutured using an absorbable surgery wire, before closing the skin incision with wound clips. The experiment was designed to infuse 5- μ g/kg body wt LPS per day (from *Escherichia coli* O111:B4 L2630, Sigma-Aldrich) for 4 weeks. For vehicle groups, the mini-pump was filled with PBS instead of LPS. Sham mice (nephrectomized, sodium citrate buffer injection) were also treated with PBS or LPS.

IL-17 Antibody Administration

Four weeks after the STZ administration, WT diabetic mice were given i.p. neutralizing IL-17A monoclonal antibody (clone 17F3, BioXCell) or IgG1 isotype control (BE0083, BioXCell) at a dose of 0.15 mg per animal, twice weekly until week 16. Sham mice (nephrectomized, sodium citrate buffer injection) were also treated with the IL-17A antibody or IgG1 isotype control.

Human Intestinal Epithelial Cells

The human intestinal epithelial cell (IEC) line, which was isolated from the human fetal small intestine, was purchased from American Type Culture Collection. It was cultured in Opti-MEM medium containing 5% FBS (Sigma), 10 mM HEPES (Dojindo), 10 mM GlutaMAX (Gibco), and 10 ng/ml EGF (BioLegend).

Bone Marrow-Derived Macrophage Experiments

Bone marrow-derived macrophages (BMDMs) were obtained from WT or MAVS KO mice (6–12 weeks), and the indicated experiments were performed as previously described.^{26,28} The details are given in Supplemental Materials and Methods.

T Cell Isolation and T Cell-BMDM Coculture

CD4⁺ T cells were isolated and cocultured with BMDMs as described in Supplemental Materials and Methods.

Macrophage Sorting

Macrophages were isolated from WT sham and diabetic kidneys using FACS Aria Fusion. The detailed procedure is described in Supplemental Materials and Methods.

Primary Tubular Epithelial Cells

Mouse kidney tubular epithelial cells (TECs) were isolated and cultured as described previously.²⁹ The glucose concentration was controlled at 5.6-mM D-glucose.

Glomerular Endothelial Cells, Mesangial Cells, and Podocytes Cultures

C57BL/6 mouse primary kidney glomerular endothelial cells (GECs) were purchased from Cell Biologics and cultured on gelatin-coated plates with Cell Biologics' Culture Complete Growth Medium (M1168). A mesangial cell line (SV40 MES 13) was obtained from American Type Culture Collection and grown in DMEM (Gibco) with 10% FBS (Sigma-Aldrich) and 1% P/S (FUJIFILM). A conditionally immortalized murine podocyte cell line was cultured and differentiated as previously described.³⁰ For siRNA transfection, cell stimulation, and cell death assay, further details are provided in Supplemental Materials and Methods.

DNA extraction, RNA extraction, quantification of 16S rDNA and *Klebsiella oxytoca*, and real-time quantitative PCR are detailed in Supplemental Materials and Methods. All primers used in this study are listed in Supplemental Table 1.

Statistical Analyses

The results were expressed as median \pm IQR, and determined using SPSS Statistics (version 23, IBM) and Prism 9.0 software. Statistical analysis was performed using the Mann-Whitney *U* test. *P* values <0.05 were considered significant.

RESULTS

MAVS^{-/-} Drives Injury under Diabetic Conditions

WT and MAVS KO mice showed a similar increase in blood glucose levels and blood pressure and decrease of body weight after STZ administration (Supplemental Figure 1). The tubular injury was evaluated using the kidney injury marker (KIM)-1 staining. The expression of KIM-1 was detected from 9 weeks after STZ injection. The diabetic MAVS KO mice exhibited an increasing KIM-1 intensity compared with WT diabetic mice at 18 weeks of diabetes (Figure 1, A and B). Urinary NGAL levels were higher in MAVS KO diabetic mice at 10 and 18 weeks after STZ injection (Figure 1C). We checked the presence of immune cells including F4/80⁺, CD3⁺, B220⁺, and Gr-1⁺ in the kidney. F4/80⁺ and CD3⁺ are the most

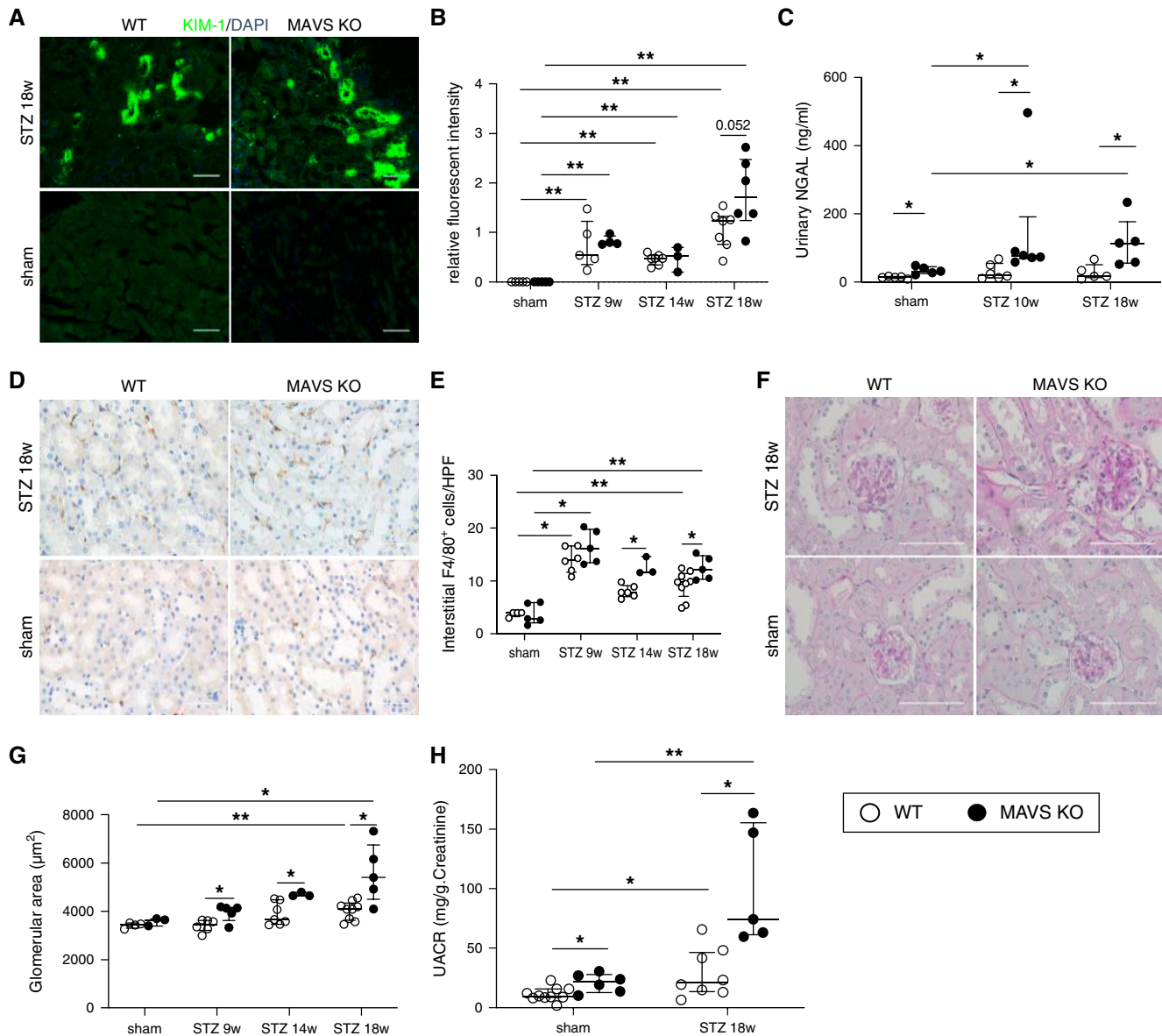


Figure 1. MAVS deficiency promotes kidney injury in diabetic condition. (A and B) Immunofluorescence analysis of KIM-1, a marker for tubule injury (magnification, $\times 200$; scale bar, 50 μm). (C) NGAL concentration in the urine. (D and E) Representative kidney histology showing interstitial F4/80 macrophage infiltration (magnification, $\times 400$; scale bar, 50 μm). (F and G) Increase in the glomerular area (magnification, $\times 400$; scale bar, 100 μm). (H) Urinary albumin excretion (UACR) is normalized to creatinine level. Data are shown as median \pm IQR; * $P < 0.05$, ** $P < 0.01$.

abundant immune cells and increased in diabetic kidneys (Supplemental Figure 2, A and B). Especially, the interstitial accumulation of F4/80 cells was also higher in MAVS KO diabetic mice (Figure 1, D and E). Glomerular damage was also induced with an increase in the glomerular area, hypercellularity, and mesangial matrix expansion, and a reduction in the number of WT-1⁺ cells (a podocyte marker), especially in MAVS KO diabetic mice (Figure 1, F and G; Supplemental Figure 2, C–F). Serum creatinine levels did not change in diabetic mice (Supplemental Figure 2G). Moreover, the diabetic MAVS KO mice exhibited higher levels of albuminuria

compared with diabetic WT mice at 18 weeks after STZ injection (Figure 1H).

MAVS Expression in Kidney Cells under Diabetic Conditions

Next, we examined the MAVS expression in the kidney cells, including tubular cells and macrophages. Immunohistochemistry staining showed a marked increase in MAVS expression in tubules from 8 weeks in diabetic kidneys (Supplemental Figure 3, A and B). Macrophages (CD45⁺CD11b⁺F4/80⁺ cells) were isolated from sham and

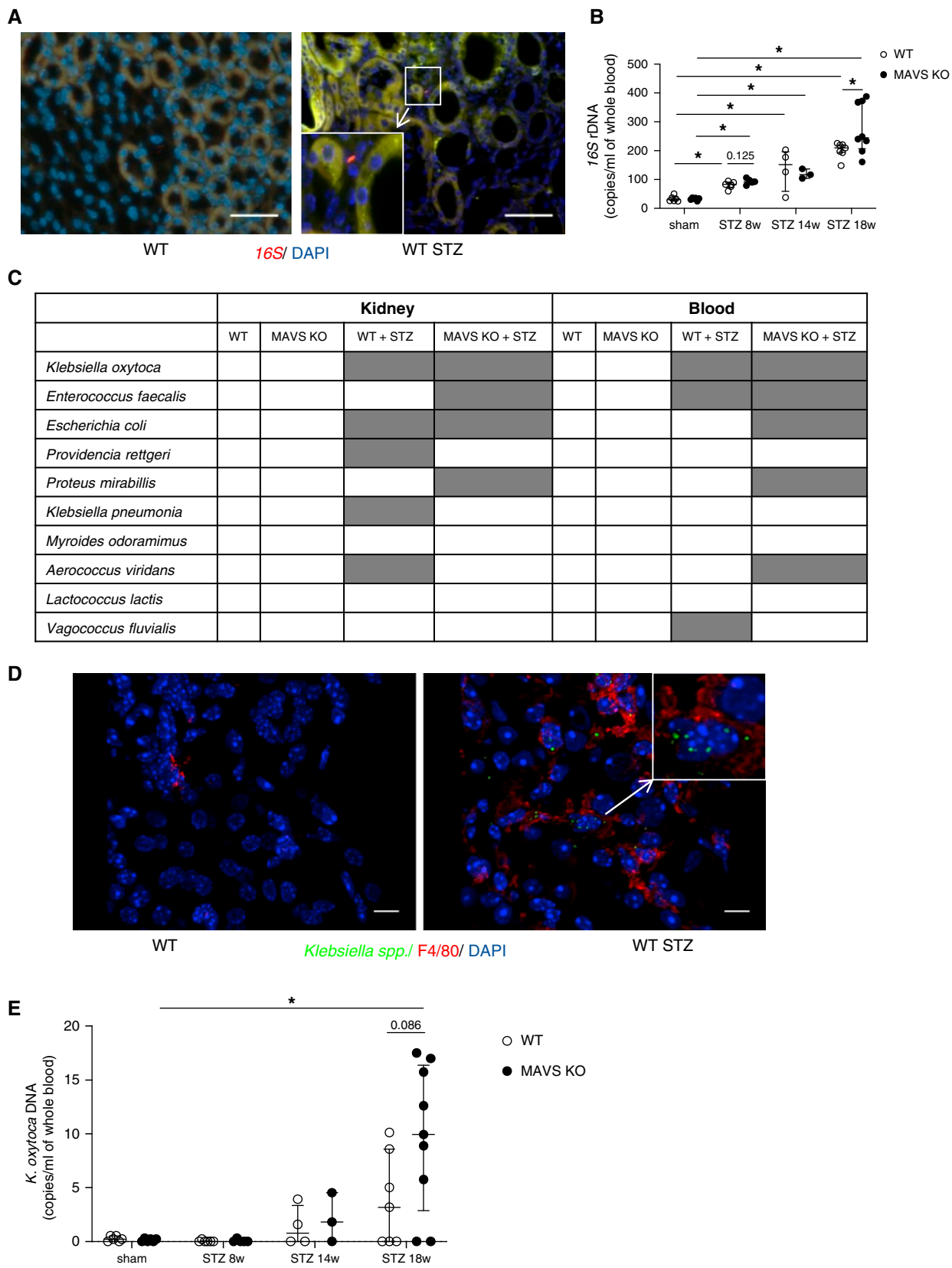


Figure 2. Detection of intestinal bacteria including *K. oxytoca* in the blood and kidney of diabetic mice. (A) Bacterial 16S in kidney sections by FISH experiment. (B) 16S rDNA quantification in the blood. (C) Bacterial strains in the kidney and blood culture.

Figure 2. (Continued) (D) Detection of *Klebsiella* spp. in the kidney of diabetic mice using immunofluorescence staining. (E) *K. oxytoca* DNA quantification in the blood. Data are shown as median \pm IQR; *P<0.05.

diabetic kidneys (Supplemental Figure 3C). Although *Mavs* mRNA expression was not changed, the mRNA expression of *Rig-I*, *Mda-5*, *Traf-3*, and *Traf-6* was slightly upregulated in diabetic macrophages compared with control macrophages (Supplemental Figure 3D).

Presence of Gut Bacteria in Circulation and Kidney in Diabetic Conditions

Fluorescent 16S rRNA-targeted probes were used to detect bacteria in the interstitium of the control and diabetic kidney (Figure 2A). We detected positive signals only in diabetic kidneys. The 16S rRNA copies increased in diabetic mice from 8 weeks after STZ injection and were higher in MAVS KO diabetic mice (Figure 2B). Live bacteria were cultured and isolated from various tissues, including the mesenteric lymph nodes, spleen, kidney, and blood. Bacteria only grew from diabetic samples. Matrix-assisted laser desorption ionization time-of-flight mass spectrometry profiling of these bacteria revealed that most bacteria were aerobic and enteric species (Figure 2C, Supplemental Figure 4). The mesenteric lymph nodes showed high bacterial diversity. *K. oxytoca* was identified in all organs. Immunofluorescence staining revealed that *Klebsiella* spp. overlapped with F4/80⁺ macrophages of the diabetic kidney (Figure 2D). *K. oxytoca* DNA was detected in blood from 14 weeks of diabetes, especially in MAVS KO diabetic mice (Figure 2E). These data demonstrated the presence of live bacteria in different tissues of diabetic mice with the abundant distribution of *K. oxytoca* including in the kidney.

Hyperglycemia Impairs Intestinal Permeability and Induces an Inflammatory State

Considering that most bacteria were identified to belong to enteric bacteria, we assumed that the intestinal barrier would be damaged. Immunofluorescence staining showed that tight junction protein zonula occludens (ZO)-1 was significantly decreased in intestines and colon from 8 weeks of diabetes, especially in MAVS KO mice (Figure 3, A–C). The function of the intestinal barrier was evaluated by determining orally administered FITC-dextran in the circulation and urine. Three hours after oral FITC-dextran administration, FITC⁺ CD11b⁺CD45⁺ cells were identified in the kidney, suggesting that intestinal phagocytes could take up and transport FITC-dextran macromolecules to the kidney (Figure 3D). Higher FITC intensity was detected in the serum at 8 weeks and urine at 18 weeks of diabetic MAVS KO mice compared with that of control diabetic mice (Figure 3, E and F). Then, we analyzed immune condition in the intestinal environment. We observed an upward trend in *Roryt/Foxp3*

mRNA expression in the lamina propria, Peyer's patches, and mesenteric lymph nodes (Figure 4, A–C) in diabetic MAVS KO mice. *T-bet* and *GATA-3* mRNA expression remained unchanged (Supplemental Figure 5). *Il-17* mRNA levels were higher in the epithelium and Peyer's patch of diabetic MAVS KO mice (Figure 4, D and E). Moreover, the number of IL-17-positive cells increased in the Peyer's patch of diabetic MAVS KO mice (Figure 4, F and G). Serum IL-17 levels also increased in diabetic mice, notably in MAVS KO diabetic mice with the peak at 14 weeks after STZ injection (Figure 4H).

Junctional Integrity Is Impaired in IECs

To determine whether glucose levels affect the intestinal epithelial barrier, we stimulated human IECs using high glucose with or without MAVS siRNA. Under high glucose exposure, both *Zo-1* mRNA (Supplemental Figure 6A) and ZO-1 protein levels (Supplemental Figure 6, B and C) were decreased, especially under the MAVS knockdown condition. Levels of the inflammatory cytokine *Il-6* increased under high glucose and *K. oxytoca* stimulation and were more prominent in MAVS knockdown cells (Supplemental Figure 6D). Moreover, *Zo-1* mRNA expression significantly decreased under IL-6 or IL-17 stimulation (Supplemental Figure 6E). These results demonstrated that glucose concentration and inflammatory cytokines (IL-6 and IL-17) directly affect barrier function.

K. oxytoca Supernatant and IL-17 Induce the Expression of KIM-1 in Primary TECs

To evaluate the pathogenesis of *K. oxytoca* to the kidney, primary TECs were stimulated with the *K. oxytoca* supernatant. We found that the *K. oxytoca* supernatant was sufficient to induce *Kim-1* gene expression (Figure 5A) in TECs, and this was higher in MAVS KO TECs than WT TECs. Immunofluorescence staining indicated a dramatically increased number of IL-17⁺ cells in the diabetic kidney over time, especially under MAVS-deficient conditions (Figure 6A). Furthermore, IL-17-stimulated TECs upregulated *Kim-1*, *Mcp-1/Ccl2*, and *Il-6* expression levels. This expression level was higher in MAVS KO TECs than WT TECs (Figure 6, B–D). We also found that both Stat3 and ERK1/2 were phosphorylated after treatment with the *K. oxytoca* supernatant (Figure 5B) or IL-17 (Figure 6E). MAVS KO TECs exhibited more robust Stat3 and ERK1/2 phosphorylation than WT TECs after 15 minutes of *K. oxytoca* supernatant stimulation (Figure 5, C and D) and 5 minutes of IL-17 stimulation (Figure 6, F–H). *K. oxytoca*-isolated RNA activated MAVS pathways with the increase

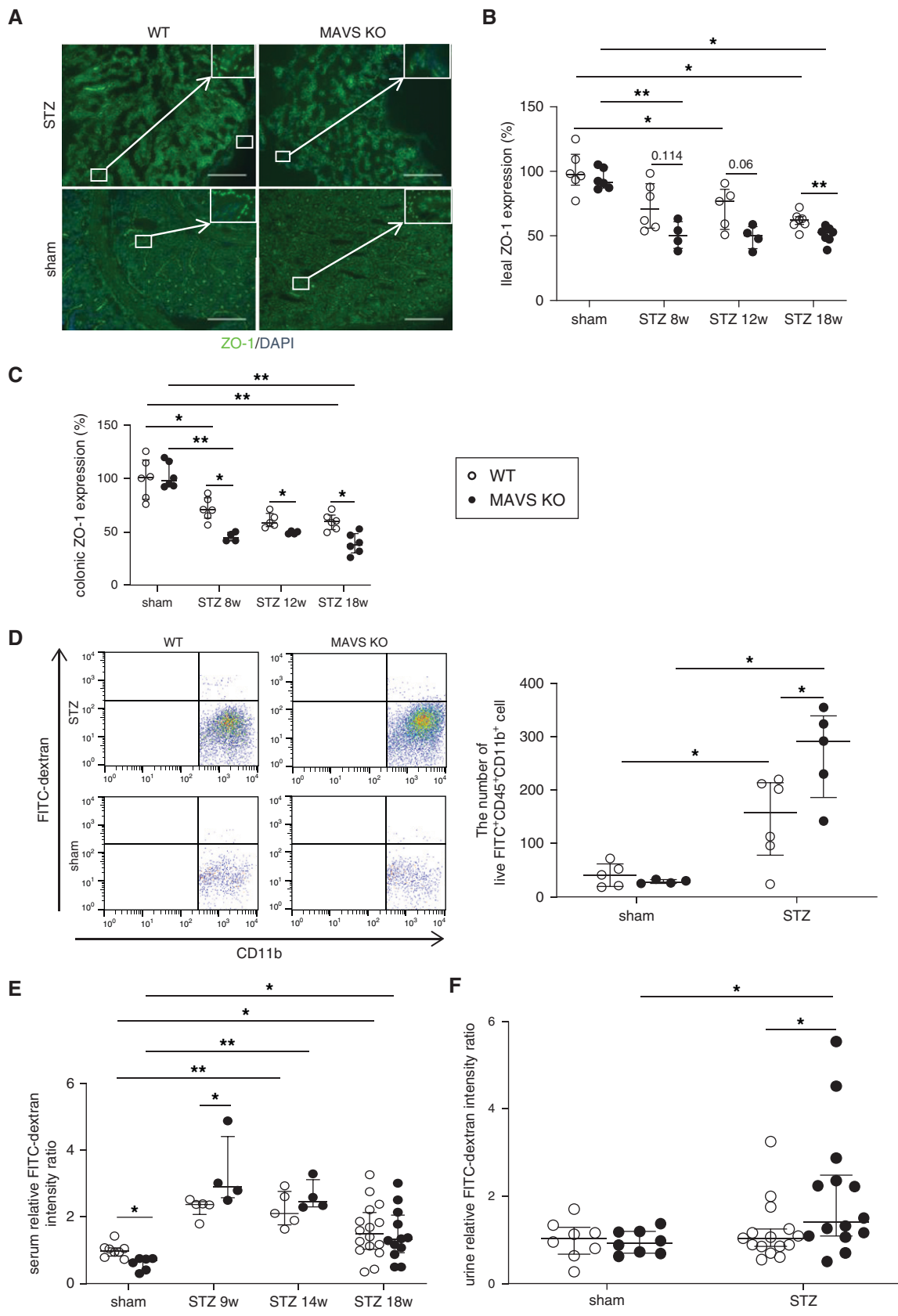


Figure 3.

Figure 3. Hyperglycemia induces the formation of a “leaky gut.” (A) Ileal ZO-1 staining (magnification, $\times 200$; scale bar, 50 μm) and relative quantification of (B) an ileal section and (C) a colon section. (D) Mice were fasted for 4 hours and gavaged with FITC-dextran 4 kDa. Flow cytometry showed the number of live FITC $^+$ CD11b $^+$ CD45 $^+$ cells in the kidney at 18 weeks after STZ injection. FITC intensity was measured in (E) serum and (F) urine. Data are shown as median \pm IQR; * $P<0.05$, ** $P<0.01$.

of *Rig-I*, *Mda-5*, *Mavs*, *Traf-3*, and *Traf-6* mRNA expression resulting in the production of *Kim-1*, *Mcp-1*, and *Il-6* (Figure 5E, Supplemental Figure 7).

BMDMs Were Activated and Impaired Function under Diabetic Conditions

Short-term high glucose conditions induced MAVS aggregation (Supplemental Figure 8A), suggesting that the MAVS signal was activated in BMDMs. *K. oxytoca* supernatant stimulation increased the levels of *Il-6*, *Il-1 β* , *Il-23p19*, *Mcp-1*, and *Tnf- α* mRNAs, especially in MAVS KO macrophages (Figure 7), indicating more severe inflammation under the MAVS-deficient condition. *K. oxytoca*

supernatant-activated BMDMs induced Th17 differentiation and *Il-17* gene upregulation (Supplemental Figure 8B). Moreover, macrophages generated under long-term high glucose conditions had impaired bactericidal ability due to reduced phagocytosis and intracellular killing of live *K. oxytoca* compared with BMDMs under normal glucose or osmotic conditions (Supplemental Figure 8, C and D).

Effects of *K. oxytoca* Supernatant and IL-17 on Glomerular Cells

Next, we evaluated the involvement of MAVS signaling in GECs, mesangial cells, and podocytes stimulated with *K. oxytoca* and IL-17. In GECs, *K. oxytoca* RNA stimulation

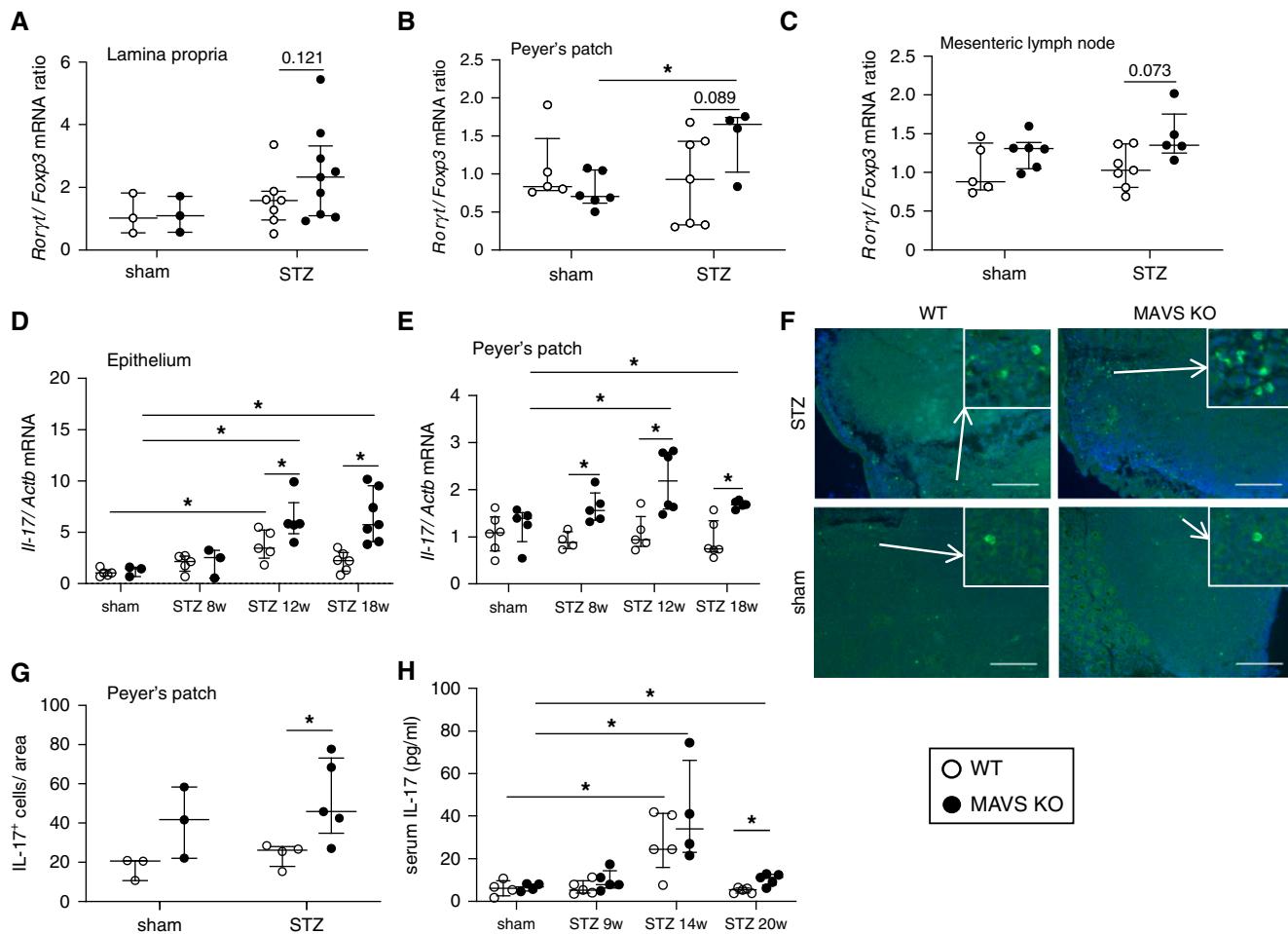


Figure 4. Hyperglycemia induced an inflammatory state in the intestine. *Rorγt*/*Foxp3* mRNA expression normalized with β -actin in (A) the lamina propria, (B) Peyer's patch, and (C) mesenteric lymph nodes at 18 weeks after STZ injection. *Il-17* mRNA expression over 18 weeks in (D) the ileal epithelium and (E) Peyer's patch. (F) IL-17 staining and (G) quantification in Peyer's patch (magnification, $\times 200$; scale bar, 50 μm) at 18 weeks of diabetes. (H) IL-17 levels in the serum. Data are shown as median \pm IQR; * $P<0.05$, ** $P<0.01$.

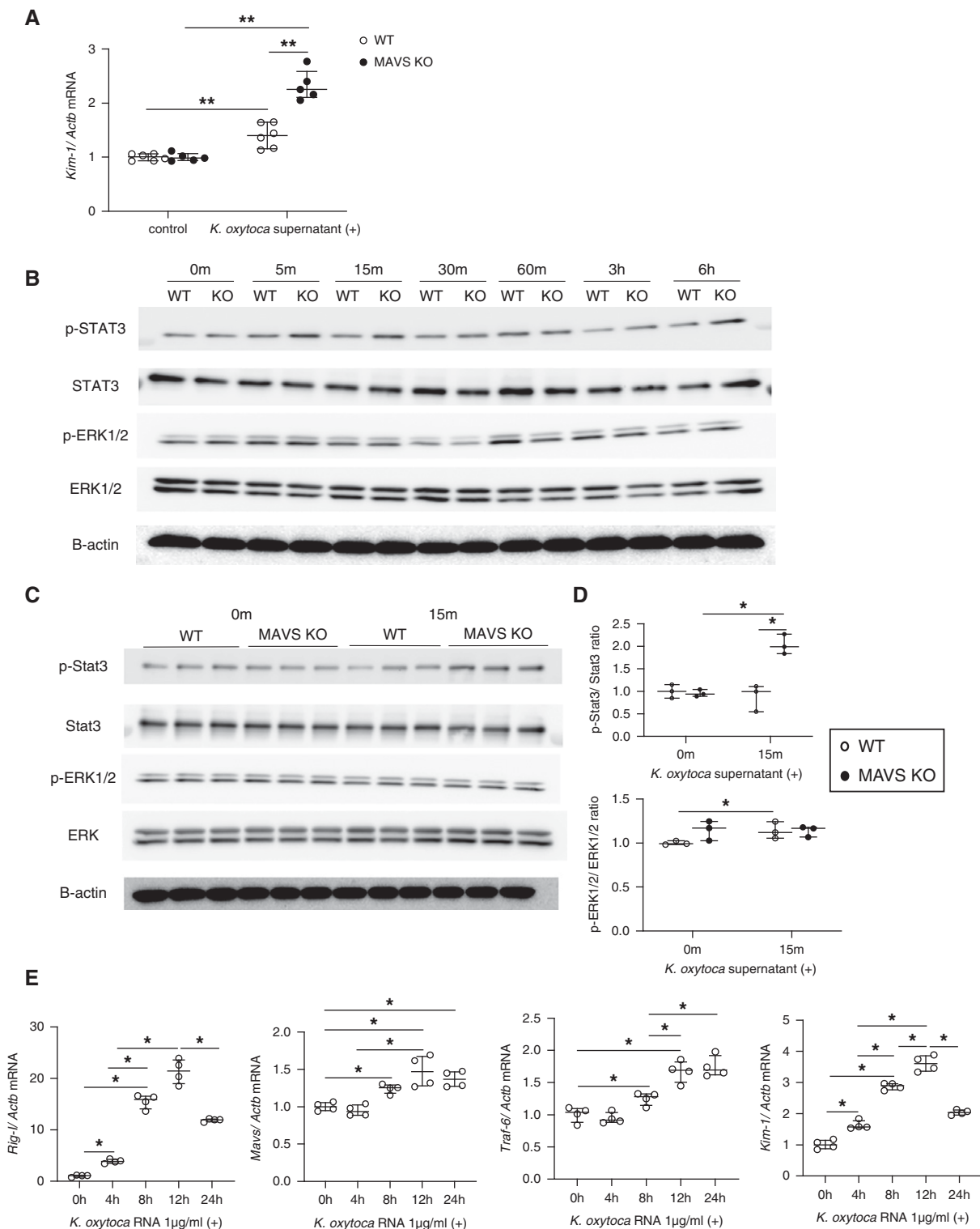


Figure 5. Effect of the *K. oxytoca* supernatant on primary TECs. (A) *Kim-1* mRNA expression after treatment with the *K. oxytoca* supernatant (1:20) for 24 hours. (B) Western blot analysis of phospho-Stat3, total Stat3, phospho-ERK1/2, and total ERK1/2 in WT and MAVS KO TECs after *K. oxytoca* supernatant stimulation (1:20) at different time points. (C and D) Western blot analysis and densitometric quantification of phospho-Stat3, total Stat3, phospho-ERK1/2, and total ERK1/2 in WT and MAVS KO TECs after *K. oxytoca* supernatant stimulation (1:20) at the indicated time. (E) Upregulation of *Rig-I*, *Mavs*, *Traf-6*, and *Kim-1* mRNA was shown under *K. oxytoca* RNA transfection. Data are shown as median±IQR; *P<0.05, **P<0.01.

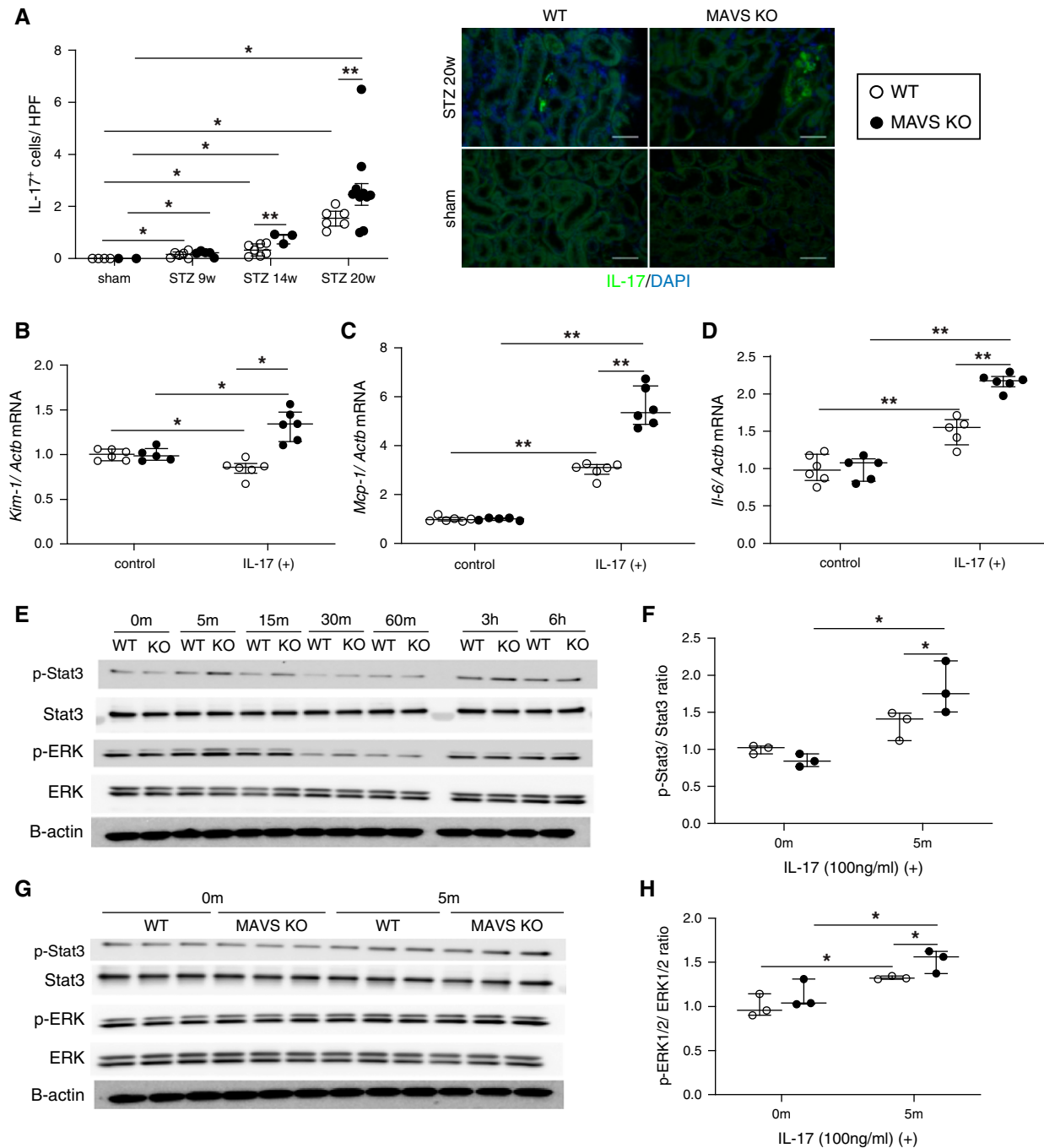


Figure 6. Change in IL-17 levels in diabetic mice and the effect of IL-17 on primary TECs. (A) IL-17 staining (magnification, $\times 400$; scale bar, 100 μ m) and quantification in the kidney. Levels of (B) *Kim-1*, (C) *Mcp-1*, and (D) *Il-6* mRNA under IL-17 stimulation (100 ng/ml) for 24 hours. (E) Western blot analysis of phospho-Stat3, total Stat3, phospho-ERK1/2, and total ERK1/2 in WT and MAVS KO TECs after IL-17 stimulation (100 ng/ml) at different time points. (F–H) Western blot analysis and densitometric quantification of phospho-Stat3, total Stat3, phospho-ERK1/2, and total ERK1/2 in WT and MAVS KO TECs after IL-17 stimulation (100 ng/ml) at the indicated time. Data are shown as median \pm IQR; * $P < 0.05$, ** $P < 0.01$.

increased the gene expression of *Rig-I*, *Mda-5*, *Mavs*, *Traf-3*, and *Traf-6*. GECs were also activated via the upregulation of *E-selectin*, *P-selectin*, and *Il-6* genes (Supplemental Figure 9). However, MAVS inhibition increased the gene expression of

activation markers on GECs under *K. oxytoca* supernatant stimulation, and IL-17 stimulation did not induce the upregulation of these genes (Supplemental Figure 10). In mesangial cells, *K. oxytoca* supernatant and IL-17 induced the expression

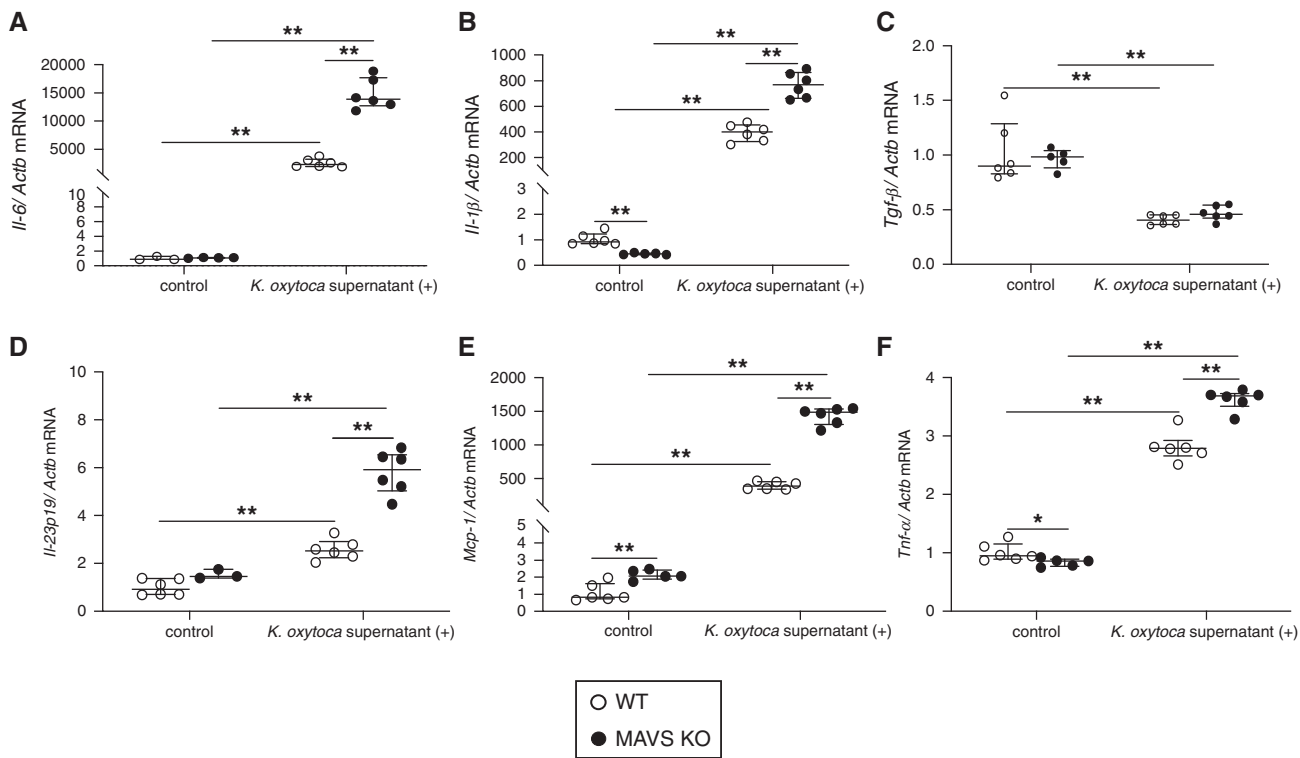


Figure 7. Effects of *K. oxytoca* supernatant to BMDMs. Proinflammatory cytokines, namely (A) *Il-6*, (B) *Il-1 β* , (C) *Tgf- β* , (D) *Il-23p19*, (E) *Mcp-1*, and (F) *Tnf- α* were expressed under the *K. oxytoca* supernatant (1:100) stimulation for 24 hours. Data are shown as median \pm IQR; * $P<0.05$, ** $P<0.01$.

of inflammatory cytokines, including *Mcp-1* and *Il-6*. MAVS suppression did not affect the expressions of these genes, apart from *Mcp-1* in IL-17 stimulated cells (Supplemental Figure 11). In podocytes, whereas *K. oxytoca* supernatant and IL-17 upregulated *Mcp-1* and *Il-6* mRNA, MAVS suppression did not affect the expression of *Zo-1*, *claudin-1*, *integrin α 3 β 1* mRNA complex, *Mcp-1*, and *Il-6* (Supplemental Figure 12). Moreover, the frequencies of apoptotic and necrotic cells were not changed with MAVS inhibition in podocytes (Supplemental Figure 13).

Although Treatment with IL-17 Neutralizing Antibody Was Protective against DKD, LPS Administration Worsened Kidney Injuries in the Diabetic Model

To explore the pathogenesis of increased levels of IL-17, we administered an anti-mouse IL-17 antibody in the murine DKD model after the development of diabetes. Treatment with the anti-mouse IL-17 antibody ameliorated tubular injury, F4/80 accumulation, and glomerular damage (Figure 8, A-D).

Next, we analyzed whether the circulating bacterial-related particles would affect the progression of DKD with the administration of low-dose LPS. LPS treatment coupled with the long-term hyperglycemic condition accelerated tubular damage, interstitial F4/80 infiltration, and glomerular injuries (Figure 8, E-H).

DISCUSSION

The study of the gut-kidney axis has opened novel therapeutic avenues for the management of inflammation, kidney injury, and uremia to prevent adverse outcomes in patients with CKD.³¹ This study showed that chronic hyperglycemia leads to a “leaky gut” and an inflammatory intestine with notably IL-17 upregulation to promote the translocation of bacteria, including *K. oxytoca* and IL-17 to extraintestinal sites and blood circulation. Subsequently, bacteremia and IL-17 turn back to worsen gut dysfunction and accelerate kidney injury. The obvious renoprotective contribution of MAVS is through maintaining intestinal integrity to reduce the gut bacterial translocation and IL-17 dominant inflammation condition. Renal MAVS signaling has versatile and complex functions in the progression of DKD (Supplemental Figure 14).

In our study, mice received a combination of STZ and unilateral nephrectomy, which induces DKD effectively in the B6 mouse strain.³² Although several studies mentioned detrimental aspects of MAVS in acute tubular necrosis³³ and unilateral ureteral obstructions,³⁴ our findings revealed that systemic MAVS signaling plays a renoprotective role in DKD. The multifunction of MAVS have recently been reported in other diseases such as energy metabolism,³⁵ pulmonary fibrosis,³⁶ and colon tumor progression.³⁷ Notably, accumulating evidence

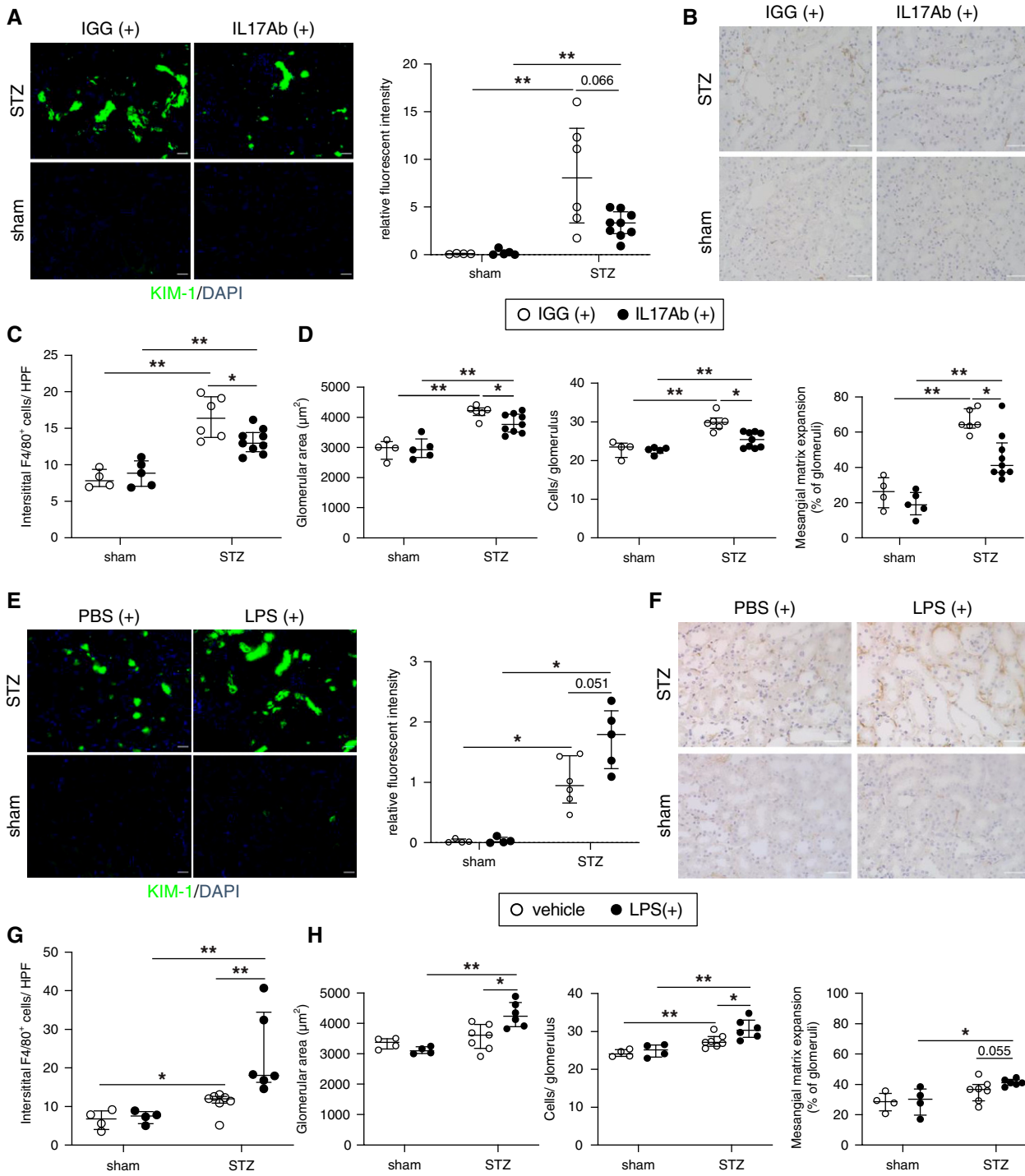


Figure 8. Neutralizing IL-17 antibody treatment ameliorates DKD whereas the administration of LPS to WT diabetic mice aggravates kidney injury. (A) Immunofluorescence analysis of KIM-1 (magnification, $\times 200$; scale bar, $50 \mu\text{m}$), (B and C) representative kidney histology showing interstitial F4/80 macrophage infiltration (magnification, $400\times$; scale bar, $50 \mu\text{m}$), and (D) pathologic glomerular analysis (glomerular area, hypercellularity, and mesangial matrix expansion) in IL-17 antibody-treated WT diabetic mice. (E) Immunofluorescence analysis of KIM-1 (magnification, $\times 200$; scale bar, $50 \mu\text{m}$), (F and G) representative kidney histology showing interstitial F4/80 macrophage infiltration (magnification, $\times 400$; scale bar, $50 \mu\text{m}$), and (H) pathologic glomerular analysis (glomerular area, hypercellularity, and mesangial matrix expansion) in LPS-treated WT diabetic mice. Data are shown as median \pm IQR; * $P < 0.05$, ** $P < 0.01$.

indicates that MAVS signaling contributes to controlling and protecting intestinal permeability.^{21–23}

A substantial body of literature has provided evidence for the role of gut-derived metabolites in the progression of diabetes.^{38–40} Our study shows aerobic enteric bacterial translocation in various tissues in diabetic mice. *K. oxytoca*, which was identified in all organs, is a member of the Enterobacteriaceae family, an opportunistic pathogen, associated with infections in hospitalized patients.⁴¹ Oral treatment with *K. oxytoca* disturbed the gut microbiome population, increased gut membrane permeability, and induced neuroinflammation and anxiety in mice.¹⁵ Consistent with our findings, the translocation of gut commensal bacteria has been reported in various diseases including diabetes.^{12,39,42,43}

In animal models exhibiting damage to the mucosal epithelium, indigenous bacteria translocate between epithelial cells into circulation.⁴⁴ ZO-1 is a cytoskeletal linker phosphoprotein that plays a key role in bringing several components together and connecting tight junction proteins to the cytoskeleton.⁴⁵ Thaiss *et al.* reported that hyperglycemia affected the integrity of tight (ZO-1) and adherence (E-cadherin) junction, then led to barrier disruption.¹³ In our study, decreased expression of ZO-1 contributed to an increase in gut permeability, in *in vivo* diabetic mice and in *in vitro* high glucose-stimulated IECs. Moreover, the role of MAVS signaling in maintaining intestinal barrier integrity was confirmed in diabetes.

Intestinal inflammation was also evoked. We observed a Th17-dominant condition in diabetic MAVS KO mice. *K. oxytoca*-activated macrophages were able to induce Th17 differentiation and IL-17 production dominant other T helper cells. Although the underlying mechanisms are unclear, studies have shown elevated IL-17 production under MAVS-deficient conditions of viral infection or allergy.^{21,46} Similar to other studies,^{47–49} we revealed that proinflammatory cytokines (IL-6, IL-17) turned back to control the tight junction structure, then accelerated gut barrier damage. So, the presence of a “leaky gut” and Th17-inflamed intestine promoted systemic enteric bacterial translocation and elevated IL-17 in diabetes. In addition to intestinal inflammation, liver injury, which is caused by gut-derived bacteria thorough portal vein, contributes to systemic inflammation in some liver diseases.^{50,51} Gut-derived *K. pneumonia* could induce Th17 inflammation within the liver in primary sclerosing cholangitis.⁵²

MAVS expression was observed most prominently in tubules and upregulated in the diabetic kidneys. In addition to virus-derived RNA, recent evidence suggests that RIG-I signaling may also play a role in the detection of bacterial pathogens, depending on the particular pathogen and host cell.^{19,20,53,54} Our study showed that *K. oxytoca* RNA could directly induce the RIG-I/MDA-5-MAVS-TRAF-3/TRAF-6 axis, leading to the production of KIM-1 in renal cells.

Surprisingly, MAVS inhibition increased *Kim-1* gene expression. This finding prompted us to explore the effect of MAVS on KIM-1-related signaling pathways such as Stat3

and ERK1/2.^{55–57} Both Stat3 and ERK1/2 signaling were activated under *K. oxytoca* supernatant and IL-17 stimulation, and a stronger activation was observed in MAVS KO TECs. These results indicate that MAVS has an inhibitory effect on the KIM-1-related signaling pathway, which results in reduced KIM-1 production. Further studies are needed to clarify the mechanism of Stat3 and ERK1/2 regulation by MAVS. In other kidney cells, MAVS was shown to play ambiguous roles in *in vitro* studies. Nevertheless, MAVS KO diabetic mice showed more severe glomerular and tubular injuries than WT diabetic mice. Given that the interaction between different cell types with multiple stimulators contributes to the pathogenesis of diabetic kidney injury, MAVS may play various roles within each microenvironment of the kidney, with or without diabetic conditions.

In mice with DKD, circulating bacterial-associated molecules and IL-17 made a significant contribution to renal injuries. A persistent low-grade LPS hastened the progression of DKD in the murine STZ-treated model. Meanwhile, the neutralization of IL-17 by antibody treatment improved both glomerular and tubular injuries in diabetic mice. Therefore, the control and maintenance of intestinal homeostasis could be a novel therapeutic target in DKD.

In conclusion, this study sheds light on the interaction between intestinal integrity, MAVS deficiency, and DKD. Controlling intestinal homeostasis through MAVS signaling would be a novel therapeutic target in DKD.

DISCLOSURES

K. Asanuma reports honoraria with AstraZeneca, Daiichi Sankyo, and Kyowa Hakko Kirin. K. Matsushima reports research funding from IDAC Theranostics, ImmunoGeneTeqs, Kyowa Hakko Kirin, and Ono Pharmaceutical. T. Wada reports research funding with Chugai Pharmaceutical, Kyowa Hakko Kirin, and Shiseido; and honoraria with Kyowa Hakko Kirin. All remaining authors have nothing to disclose.

FUNDING

This work was supported by the Japan Society for the Promotion of Science Grant-in-Aid for Scientific Research on Innovative Areas program (Inflammation Cellular Sociology: 17H06394 to K. Furuchi, Y. Iwata, N. Sakai, and T. Wada) and KAKENHI (18K08426 and 21K08224 to Y. Iwata) and by Kanazawa University SAKIGAKE project 2020 (to Y. Iwata).

AUTHOR CONTRIBUTIONS

Y. Iwata, H.T. Linh, and T. Wada designed and performed the experiments and wrote the manuscript; Y. Sakai-Takemori and Y. Senda performed bacterial culture; K. Furuchi, A. Hara, S. Kitajima, Y. Nakade, T. Minami, T. Miyagawa, S. Nakagawa-Yoneda, M. Oshima, H. Ogura, M. Shimizu, K. Sato, N. Sakai, T. Toyama, and Y. Yamamura supported the mouse experiments; K. Asanuma and H. Yamada supported the podocyte experiments; and K. Matsushima and T. Wada supervised the work.

DATA SHARING STATEMENT

All data is included in the manuscript and/or supporting materials.

SUPPLEMENTAL MATERIAL

This article contains the following supplemental material online at http://jasn.asnjournals.org/lookup/suppl/doi:10.1681/ASN.2021060843/-/DC_Supplemental:

Supplemental Materials and Methods.

Supplemental Figure 1. WT and MAVS KO mice developed equivalent degrees of hyperglycemia.

Supplemental Figure 2. Mitochondrial antiviral signaling protein (MAVS) deficiency promotes glomerular injury in diabetic conditions.

Supplemental Figure 3. MAVS expression in the kidney and macrophages of WT diabetic mice.

Supplemental Figure 4. Bacterial strains in the spleen and mesenteric lymph node culture.

Supplemental Figure 5. An intestinal inflammatory condition in the sham and diabetic mice.

Supplemental Figure 6. Experiments with human intestinal epithelial cells (IECs).

Supplemental Figure 7. *K. oxytoca* activates RIG-I/MDA-5-MAVS-TRAF-3/TRAF-6 signaling pathway in TECs.

Supplemental Figure 8. The dysfunction of bone marrow-derived macrophages (BMDMs).

Supplemental Figure 9. *K. oxytoca* supernatant activates RIG-I/MDA-5-MAVS-TRAF-3/TRAF-6 signaling pathway in glomerular endothelial cells (GECs).

Supplemental Figure 10. The effect of *K. oxytoca* supernatant and IL-17 on glomerular endothelial cells (GECs) under normal and MAVS knockdown condition.

Supplemental Figure 11. The effect of *K. oxytoca* supernatant and IL-17 on mesangial cells under normal and MAVS knockdown condition.

Supplemental Figure 12. The effect of *K. oxytoca* and IL-17 on immortalized conditional culture podocytes.

Supplemental Figure 13. The effect of *K. oxytoca* and IL-17 to cell death on immortalized conditional culture podocytes.

Supplemental Figure 14. Schematic graphic.

Supplemental Table 1. List of primers used for qPCR.

REFERENCES

- Locatelli F, Pozzani P, Del Vecchio L: Renal replacement therapy in patients with diabetes and end-stage renal disease. *J Am Soc Nephrol* 15[Suppl 1]: S25–S29, 2004
- Schieber AM, Lee YM, Chang MW, Leblanc M, Collins B, Downes M, et al.: Disease tolerance mediated by microbiome *E. coli* involves inflammasome and IGF-1 signaling. *Science* 350: 558–563, 2015
- Zhu S, Jiang Y, Xu K, Cui M, Ye W, Zhao G, et al.: The progress of gut microbiome research related to brain disorders. *J Neuroinflammation* 17: 25, 2020
- Kikuchi K, Saigusa D, Kanemitsu Y, Matsumoto Y, Thanai P, Suzuki N, et al.: Gut microbiome-derived phenyl sulfate contributes to albuminuria in diabetic kidney disease. *Nat Commun* 10: 1835, 2019
- Musket MH, Smits MM, Morsink LM, Diamant M: The gut-renal axis: Do incretin-based agents confer renoprotection in diabetes? *Nat Rev Nephrol* 10: 88–103, 2014
- Wu IW, Hsu KH, Lee CC, Sun CY, Hsu HJ, Tsai CJ, et al.: p-Cresyl sulphate and indoxyl sulphate predict progression of chronic kidney disease. *Nephrol Dial Transplant* 26: 938–947, 2011
- Nakade Y, Iwata Y, Furuichi K, Mita M, Hamase K, Konno R, et al.: Gut microbiota-derived D-serine protects against acute kidney injury. *JCI Insight* 3: e97957, 2018
- Kawashima T, Kosaka A, Yan H, Guo Z, Uchiyama R, Fukui R, et al.: Double-stranded RNA of intestinal commensals but not pathogenic bacteria triggers production of protective interferon-β. *Immunity* 38: 1187–1197, 2013
- Hooper LV, Gordon JI: Commensal host-bacterial relationships in the gut. *Science* 292: 1115–1118, 2001
- Ichinohe T, Pang IK, Kumamoto Y, Peaper DR, Ho JH, Murray TS, et al.: Microbiota regulates immune defense against respiratory tract influenza A virus infection. *Proc Natl Acad Sci U S A* 108: 5354–5359, 2011
- Abt MC, Osborne LC, Monticelli LA, Doering TA, Alenghat T, Sonnenberg GF, et al.: Commensal bacteria calibrate the activation threshold of innate antiviral immunity. *Immunity* 37: 158–170, 2012
- Shah NB, Allegretti AS, Nigwekar SU, Kalim S, Zhao S, Lelouvier B, et al.: Blood microbiome profile in CKD: A pilot study. *Clin J Am Soc Nephrol* 14: 692–701, 2019
- Thaiss CA, Levy M, Groshev I, Zheng D, Soffer E, Blacher E, et al.: Hyperglycemia drives intestinal barrier dysfunction and risk for enteric infection. *Science* 359: 1376–1383, 2018
- Cani PD, Bibiloni R, Knauf C, Waget A, Neyrinck AM, Delzenne NM, et al.: Changes in gut microbiota control metabolic endotoxemia-induced inflammation in high-fat diet-induced obesity and diabetes in mice. *Diabetes* 57: 1470–1481, 2008
- Jang H-M, Lee H-J, Jang S-E, Han MJ, Kim D-H: Evidence for interplay among antibacterial-induced gut microbiota disturbance, neuro-inflammation, and anxiety in mice. *Mucosal Immunol* 11: 1386–1397, 2018
- Vaarala O, Atkinson MA, Neu J: The “perfect storm” for type 1 diabetes: The complex interplay between intestinal microbiota, gut permeability, and mucosal immunity. *Diabetes* 57: 2555–2562, 2008
- Schlee M, Hartmann G: Discriminating self from non-self in nucleic acid sensing. *Nat Rev Immunol* 16: 566–580, 2016
- Seth RB, Sun L, Ea C-K, Chen ZJ: Identification and characterization of MAVS, a mitochondrial antiviral signaling protein that activates NF-κappaB and IRF 3. *Cell* 122: 669–682, 2005
- Dixit E, Kagan JC: Intracellular pathogen detection by RIG-I-like receptors. *Adv Immunol* 117: 99–125, 2013
- Schmolke M, Patel JR, de Castro E, Sánchez-Aparicio MT, Uccellini MB, Miller JC, et al.: RIG-I detects mRNA of intracellular *Salmonella enterica* serovar *Typhimurium* during bacterial infection. *mBio* 5: e01006–e01014, 2014
- Plantamura E, Dzutsev A, Chamaillard M, Djebali S, Moudombi L, Boucinha L, et al.: MAVS deficiency induces gut dysbiotic microbiota conferring a proallergic phenotype. *Proc Natl Acad Sci U S A* 115: 10404–10409, 2018
- Li XD, Chiu YH, Ismail AS, Behrendt CL, Wight-Carter M, Hooper LV, et al.: Mitochondrial antiviral signaling protein (MAVS) monitors commensal bacteria and induces an immune response that prevents experimental colitis. *Proc Natl Acad Sci U S A* 108: 17390–17395, 2011
- Fischer JC, Bscheider M, Eisenkolb G, Lin C-C, Wintges A, Otten V, et al.: RIG-I/MAVS and STING signaling promote gut integrity during irradiation- and immune-mediated tissue injury. *Sci Transl Med* 9: eaag2513, 2017
- Ma J, Li YJ, Chen X, Kwan T, Chadban SJ, Wu H: Interleukin 17A promotes diabetic kidney injury. *Sci Rep* 9: 2264, 2019
- Yang L, Brooks CR, Xiao S, Sabbisetti V, Yeung MY, Hsiao L-L, et al.: KIM-1-mediated phagocytosis reduces acute injury to the kidney. *J Clin Invest* 125: 1620–1636, 2015
- Iwata Y, Boström EA, Menke J, Rabacal WA, Morel L, Wada T, et al.: Aberrant macrophages mediate defective kidney repair that triggers nephritis in lupus-susceptible mice. *J Immunol* 188: 4568–4580, 2012
- Miyake T, Sakai N, Tamai A, Sato K, Kamikawa Y, Miyagawa T, et al.: Trehalose ameliorates peritoneal fibrosis by promoting Snail

- degradation and inhibiting mesothelial-to-mesenchymal transition in mesothelial cells. *Sci Rep* 10: 14292, 2020
28. Pavlou S, Lindsay J, Ingram R, Xu H, Chen M: Sustained high glucose exposure sensitizes macrophage responses to cytokine stimuli but reduces their phagocytic activity. *BMC Immunol* 19: 24, 2018
 29. Faust J, Menke J, Kriegsmann J, Kelley VR, Mayet WJ, Galle PR, et al.: Correlation of renal tubular epithelial cell-derived interleukin-18 up-regulation with disease activity in MRL-FasLpr mice with autoimmune lupus nephritis. *Arthritis Rheum* 46: 3083–3095, 2002
 30. Yamada H, Shirata N, Makino S, Miyake T, Trejo JAO, Yamamoto-Nonaka K, et al.: MAGI-2 orchestrates the localization of backbone proteins in the slit diaphragm of podocytes. *Kidney Int* 99: 382–395, 2021
 31. Chen YY, Chen DQ, Chen L, Liu JR, Vaziri ND, Guo Y, et al.: Microbiome-metabolome reveals the contribution of gut-kidney axis on kidney disease. *J Transl Med* 17: 5, 2019
 32. Uil M, Scantleberry AML, Butter LM, Larsen PWB, de Boer OJ, Leemans JC, et al.: Combining streptozotocin and unilateral nephrectomy is an effective method for inducing experimental diabetic nephropathy in the “resistant” C57Bl/6J mouse strain. *Sci Rep* 8: 5542, 2018
 33. Subramanian N, Natarajan K, Clatworthy MR, Wang Z, Germain RN: The adaptor MAVS promotes NLRP3 mitochondrial localization and inflammasome activation. *Cell* 153: 348–361, 2013
 34. Kim SM, Kim YG, Kim DJ, Park SH, Jeong KH, Lee YH, et al.: Inflammasome-independent role of NLRP3 mediates mitochondrial regulation in renal injury. *Front Immunol* 9: 2563, 2018
 35. Zhang W, Wang G, Xu ZG, Tu H, Hu F, Dai J, et al.: Lactate is a natural suppressor of RLR signaling by targeting MAVS. *Cell* 178: 176–189.e15, 2019
 36. Kim S-H, Lee JY, Yoon CM, Shin HJ, Lee SW, Rosas I, et al.: Mitochondrial antiviral signalling protein is crucial for the development of pulmonary fibrosis. *Eur Respir J* 57: 200652, 2021
 37. Zhang W, Gong J, Yang H, Wan L, Peng Y, Wang X, et al.: The mitochondrial protein MAVS stabilizes p53 to suppress tumorigenesis. *Cell Rep* 30: 725–738.e4, 2020
 38. Lassenius MI, Pietiläinen KH, Kaartinen K, Pussinen PJ, Syrjänen J, Forsblom C, et al.; FinnDiane Study Group: Bacterial endotoxin activity in human serum is associated with dyslipidemia, insulin resistance, obesity, and chronic inflammation. *Diabetes Care* 34: 1809–1815, 2011
 39. Pussinen PJ, Havulinna AS, Lehto M, Sundvall J, Salomaa V: Endotoxemia is associated with an increased risk of incident diabetes. *Diabetes Care* 34: 392–397, 2011
 40. Huang W, Man Y, Gao C, Zhou L, Gu J, Xu H, et al.: Short-chain fatty acids ameliorate diabetic nephropathy via GPR43-mediated inhibition of oxidative stress and NF-κB signaling. *Oxid Med Cell Longev* 2020: 4074832, 2020
 41. Validi M, Soltan-Dallal MM, Douraghi M, Fallah-Mehrabadi J, Rahimi-Foroushani A, Frohesh-Tehrani H: Identification of cytotoxin-producing *Klebsiella oxytoca* strains isolated from clinical samples with cell culture assays. *Microb Pathog* 113: 1–4, 2017
 42. Costa FR, Françozo MC, de Oliveira GG, Ignacio A, Castoldi A, Zamboni DS, et al.: Gut microbiota translocation to the pancreatic lymph nodes triggers NOD2 activation and contributes to T1D onset. *J Exp Med* 213: 1223–1239, 2016
 43. Hu J, Luo H, Wang J, Tang W, Lu J, Wu S, et al.: Enteric dysbiosis-linked gut barrier disruption triggers early renal injury induced by chronic high salt feeding in mice. *Exp Mol Med* 49: e370, 2017
 44. Berg RD: Bacterial translocation from the gastrointestinal tract. *Adv Exp Med Biol* 473: 11–30, 1999
 45. Assimakopoulos SF, Papageorgiou I, Charonis A: Enterocytes’ tight junctions: From molecules to diseases. *World J Gastrointest Pathophysiol* 2: 123–137, 2011
 46. Da Costa A, Garza E, Graham JB, Swarts JL, Soerens AG, Gale M, et al.: Extrinsic MAVS signaling is critical for Treg maintenance of Foxp3 expression following acute flavivirus infection. *Sci Rep* 7: 40720, 2017
 47. Ogawa A, Andoh A, Araki Y, Bamba T, Fujiyama Y: Neutralization of interleukin-17 aggravates dextran sulfate sodium-induced colitis in mice. *Clin Immunol* 110: 55–62, 2004
 48. Ito R, Kita M, Shin-Ya M, Kishida T, Urano A, Takada R, et al.: Involvement of IL-17A in the pathogenesis of DSS-induced colitis in mice. *Biochem Biophys Res Commun* 377: 12–16, 2008
 49. Lee JS, Tato CM, Joyce-Shaikh B, Gulen MF, Cayatte C, Chen Y, et al.: Interleukin-23-independent IL-17 production regulates intestinal epithelial permeability [published correction appears in *Immunity* 43: 1022, 2015]. *Immunity* 43: 727–738, 2015
 50. Ohtani N, Kawada N: Role of the gut-liver axis in liver inflammation, fibrosis, and cancer: A special focus on the gut microbiota relationship. *Hepatol Commun* 3: 456–470, 2019
 51. Sun J, Zhang J, Wang X, Ji F, Ronco C, Tian J, et al.: Gut-liver cross-talk in sepsis-induced liver injury. *Crit Care* 24: 614, 2020
 52. Nakamoto N, Sasaki N, Aoki R, Miyamoto K, Suda W, Teratani T, et al.: Gut pathogens underlie intestinal barrier dysfunction and liver T helper 17 cell immune response in primary sclerosing cholangitis. *Nat Microbiol* 4: 492–503, 2019
 53. Monroe KM, McWhirter SM, Vance RE: Identification of host cytosolic sensors and bacterial factors regulating the type I interferon response to *Legionella pneumophila*. *PLoS Pathog* 5: e1000665, 2009
 54. Abdullah Z, Schlee M, Roth S, Mraheil MA, Barchet W, Böttcher J, et al.: RIG-I detects infection with live *Listeria* by sensing secreted bacterial nucleic acids. *EMBO J* 31: 4153–4164, 2012
 55. Humphreys BD, Xu F, Sabbisetti V, Grgic I, Movahedi Naini S, Wang N, et al.: Chronic epithelial kidney injury molecule-1 expression causes murine kidney fibrosis. *J Clin Invest* 123: 4023–4035, 2013
 56. Ajay AK, Kim TM, Ramirez-Gonzalez V, Park PJ, Frank DA, Vaidya VS: A bioinformatics approach identifies signal transducer and activator of transcription-3 and checkpoint kinase 1 as upstream regulators of kidney injury molecule-1 after kidney injury. *J Am Soc Nephrol* 25: 105–118, 2014
 57. Collier JB, Schnellmann RG: Extracellular signal-regulated kinase 1/2 regulates mouse kidney injury molecule-1 expression physiologically and following ischemic and septic renal injury. *J Pharmacol Exp Ther* 363: 419–427, 2017

AFFILIATIONS

¹Department of Nephrology and Laboratory Medicine, Kanazawa University, Kanazawa, Japan

²Division of Infection Control, Kanazawa University Hospital, Kanazawa, Japan

³Division of Blood Purification, Kanazawa University Hospital, Kanazawa, Japan

⁴Division of Nephrology, Kanazawa Medical University School of Medicine, Kanazawa, Japan

⁵Department of Nephrology, Graduate School of Medicine, Chiba University, Chiba, Japan

⁶Division of Molecular Regulation of Inflammatory and Immune Diseases, Research Institute of Biomedical Sciences, Tokyo University of Science, Tokyo, Japan

Supplemental Material

Supplemental Table of Contents

Materials Methods Supplement

Supplemental Figure 1 WT and MAVS KO mice developed equivalent degrees of hyperglycemia.

Supplemental Figure 2 Mitochondrial antiviral signaling protein (MAVS) deficiency promotes glomerular injury in diabetic conditions.

Supplemental Figure 3 MAVS expression in the kidney and macrophages of WT diabetic mice.

Supplemental Figure 4 Bacterial strains in spleen and mesenteric lymph node culture

Supplemental Figure 5 An intestinal inflammatory condition in the sham and diabetic mice

Supplemental Figure 6 Experiments with human intestinal epithelial cells (IECs).

Supplemental Figure 7 *K. oxytoca* activates RIG-I/MDA-5–MAVS – TRAF-3/TRAF-6 signaling pathway in TECs

Supplemental Figure 8 The dysfunction of bone marrow-derived macrophages (BMDMs)

Supplemental Figure 9 *K. oxytoca* supernatant activates RIG-I/MDA-5–MAVS–TRAF-3/TRAF-6 signaling pathway in glomerular endothelial cells (GECs)

Supplemental Figure 10 The effect of *K. oxytoca* supernatant and IL-17 on glomerular endothelial cells (GECs) under normal and MAVS knockdown condition

Supplemental Figure 11 The effect of *K. oxytoca* supernatant and IL-17 on mesangial cells under normal and MAVS knockdown condition

Supplemental Figure 12 The effect of *K. oxytoca* and IL-17 on immortalized conditional culture podocytes

Supplemental Figure 13 The effect of *K. oxytoca* and IL-17 to cell death on immortalized conditional culture podocytes.

Supplemental Figure 14 Schematic graphic

Supplemental Table 1 List of primers used for qPCR

Materials and Methods Supplement

Quantification of urine albumin and creatinine

Urine albumin was quantified using the Mouse Albumin ELISA Quantification Set (Bethyl Laboratories) according to the manufacturer's instructions. Urine creatinine was measured enzymatically using LabAssayTM Creatinine (FUJIFILM).

Serum creatinine was measured by Oriental Yeast Co., Ltd (Tokyo, Japan).

Immunostaining

Paraffin-embedded tissue or frozen sections and cultured cells were fixed in 4% paraformaldehyde. After blocking with Protein blocking solution (DAKO), the samples were stained with primary antibody at 4°C overnight. The next day, sections were incubated with appropriated secondary antibody 1h at room temperature. Primary antibodies used include rabbit polyclonal anti-ZO-1 (Invitrogen, 40-2200), rabbit polyclonal anti-WT1 (C-19) (Santacruz, sc192), goat polyclonal anti-mouse kidney injury marker (KIM)-1 (R&D, AF1817), rabbit polyclonal anti-IL-17 (Abcam, ab79056), and rabbit polyclonal anti-*Klebsiella spp* (FITC) (Abcam, ab69467), MAVS (CST, #4983), rabbit anti-CD3 (Nichirei Bio, 413591), purified Rat Anti-Mouse CD45R/B220 (BD, 01121A), purified Rat Anti-Mouse Ly-6G and Ly-6C (Gr-1) (BD, 550291).

Western blot and MAVS aggregation

Total cellular lysates were extracted from cultured cells in RIPA buffer (Merck Millipore) with protease and phosphatase inhibitors (Roche). Cellular lysates were separated by sodium dodecyl sulfate-polyacrylamide gel electrophoresis (SDS-PAGE). For MAVS aggregation, lysates were run on 1.5% agarose, 0.1% SDS gel, then transferred to PVDF (Thermo Fisher Scientific). After incubation in PVDF-blocking reagent (TOYOBIO, Japan), membranes were incubated with primary antibody overnight at 4 °C followed by incubation with appropriate secondary antibodies for 1 h at room temperature. Then, membrane-derived protein bands were detected using the enhanced chemiluminescent substrate (Thermo Fisher Scientific). The used primary antibodies for Western blot include MAVS (CST, #4983), Stat3 (79D7) Rabbit mAb (CST, #4904), Phospho-Stat3 (Tyr 705) (D3A7) (D3A7) XP® Rabbit mAb (CST, #9145), p44/42 MAPK (Erk1/2) (137F5) rabbit mAb (CST, #4695), Phospho-p44/42 MAPK (Erk1/2) (Thr 202/Tyr 204) (197G2) rabbit mAb (CST, #4377), and β-actin Rabbit Ab (CST, #4967)

Intestinal permeability assay with FITC-dextran (FD) 4 kDa

Fluorescence intensity in the serum, and urine was measured at an excitation wavelength of 490 nm and emission wavelength of 510–570 nm using the GloMax®-Multi Detection System.

Flow cytometry

The kidney was collected and digested using collagenase I (1mg/ml) (Worthington Biochemical Corporation) and DNase I (200 mg/ml) (Roche). The isolated cells were resuspended in 5% FBS–PBS, stained with CD45-PE and CD11b-APC antibodies (BD Bioscience) for 30 min on ice. After washing, the stained cells were resuspended in PBS, mixed with PI (Immunostep Biotech), run on a BD FACS Calibur cytometer, and analyzed with FlowJo software.

Assessment of bacterial translocation

The spleen, kidney, and mesenteric lymph nodes were aseptically removed, minced with sterile PBS under sterile conditions, divided into two Tryptic soy broth (TSB) (Nippon Becton Dickson) liquid medium tubes, and placed in an aerobic and anaerobic incubator at 37°C. After 3 d, 10 µl of the aerobic culture medium was inoculated onto blood (Nissui), and Drigalski Lactose Agar (BTB) agar (Nippon Becton Dickson) and aerobically incubated for 24 h. Then, 10 µl of the anaerobic culture medium was streaked on BHK Brucella agar (KYOKUTO) and anaerobically incubated for 48 h. The colonies growing on the plates were identified using Bruker Matrix-assisted laser desorption/ionization-time-of-flight mass spectrometry (MALDI-TOF MS) biotype identification system.

Blood was aseptically collected, 0.5 mL of the sample was inoculated (through a safety device Vacutainer) into a BD BACTECT™ Peds Plus™ Medium (Becton Dickson), then incubated for 7 d. For bottles flagged positive, an inoculum was sub-cultured, cloned, and identified.

Bone marrow-derived macrophages (BMDMs) culture

Conditioned medium from L929 (ATCC) fibroblast cells was used as a crude source of macrophage colony-stimulating factor (M-CSF or CSF-1) for the culture of macrophages. Bone marrow cells were isolated from femurs of WT or MAVS KO mice (6–12 weeks), cultured in L929 cell-conditioned medium (RPMI 1640 (Gibco) with 20% L929 medium,

10% FBS (Sigma-Aldrich), and 1% P/S (FUJIFILM)) to separate adherent differentiated cells. Non-adherent, immature cells were removed and cultured for 3–4 days. Glucose concentration was controlled at 5.6 mM D-glucose (normal glucose [NG]), plus 25mM D-glucose (FUJIFILM) (high glucose [HG]) or 25mM L-glucose (Sigma Aldrich) (osmotic control [OSM]). For long-term exposure with NG, HG, or OSM, bone marrow cells were cultured and differentiated in different media immediately after being isolated for 7 d. For short-term exposure, bone marrow cells were cultured in NG medium, then stimulated with HG or OSM media at the indicated time.

T cell isolation and T cell–BMDMs coculture

Remove the spleen from WT mice. The plunger of a 1ml syringe was used to grin the spleen on a sterile 100 μ m cell strainer mesh in a Petri dish containing 2 ml ice-cold RPMI/FBS to obtain a single-cell suspension. Pass through all cells through a cell strainer into a 50-ml tube. Wash the cell culture strainer and dish with 5 ml of RPMI twice and combine all cells. Centrifuge the cells and remove the supernatant. Resuspend the cell pellet into 5 ml of 1X BD Pharm LyseTM lysing solution (BD Bioscience). Centrifuge the cells and re-suspend the cell pellet in 0.5% BSA, 2mM EDTA in PBS. Count the cells, then isolate CD4⁺ T cells using CD4⁺ T cell Isolation Kit (Miltenyi Biotec) as manufacturer's protocol. Isolated cells were resuspended in RPMI with 10% FBS (Sigma Aldrich), 1% P/S (FUJIFILM), 10mM Hepes (Dojindo), 1 mM Sodium Pyruvate (FUJIFILM). All procedures were performed aseptically. The purity of isolated cells was confirmed by flow cytometry over 90%.

WT BMDMs (in NG condition) were seeded on 12-well plates at 1x10⁵ cells/ well. 24 h after *K. oxytoca* supernatant stimulation, the medium was changed to fresh medium and isolated CD4⁺ T cells were added to BMDMs with a 1:1 ratio. After 72 h, T cells in the supernatant were collected and extracted RNA.

Macrophage sorting

Kidneys were isolated from mice after perfusion with cold PBS and cut into small pieces. Kidneys were digested in 5 ml of RPMI (Gibco) with 0.25 mg/ml Liberase (Gibco) and 0.2 mg/ml DNase I (Roche). After digestion, cells were passed through a 70- μ m strainer and washed once with 5% FBS-PBS. Mononuclear cells were enriched using a 65%–25% Percoll (GE Healthcare) gradient by centrifugation (1000 g for 20 min at room temperature). After Percoll enrichment, cells were washed once and resuspended in FACS buffer (PBS with

1% BSA (Sigma Aldrich), 1 mM EDTA (Nippon Gene), 25 mM Hepes (Dojindo)). For surface staining, cells were incubated with purified anti-mouse CD16/32 Fc Block (BD Bioscience, 553142) for 10 min on ice. Additional antibodies including anti-mouse CD45-PE (103106), CD11b-FITC (101206), and F4/80-APC (17-4801-80) (BD Bioscience) were then added in FACS buffer to a final volume of 100 µl at 4°C for 30 min. After staining, cells were washed twice and resuspended in FACS buffer adding 7-AAD (BioLegend), then sorted using FACS Aria Fusion. The purity was confirmed over 95%.

RNeasy Micro Kit (QIAGEN) was used to extract RNA from sorted cells.

DNA extraction

DNA from whole blood samples was extracted using the DNeasy PowerLyser Microbial kit (QIAGEN) or Nucleospin Tissue (Takara).

Droplet digital PCR

Droplet digital PCR (ddPCR) was performed using the QX200 AutoDG Droplet Digital PCR System (Bio-Rad) according to the manufacturer's protocol. Each 22 µl ddPCR reaction contained 11 µl of the 2x ddPCR SuperMix for probes (no dUTP) (Bio-Rad), template DNA, *K. oxytoca* primer, and probes (Genesig), and *16S rDNA* TaqMan primers and probes (catalog Ba04230899_s1; Applied Biosystems TaqMan Gene Expression Assays). at defined concentrations. Reactions were prepared in a semi-skirted 96-well plate (Bio-Rad). Following droplet generation on the AutoDG system, the plate was sealed with a pierceable foil heat seal (Bio-Rad) and PCR was performed on the C1000 Touch™ thermal cycler (Bio-Rad). After the PCR reaction was completed, the plate was read using a QX200 droplet reader (Bio-Rad) and then analyzed using QuantaSoft software.

siRNA transfection and stimulation experiments for cultured cells.

Human and murine siMAVS were obtained from Invitrogen and transiently transfected using Lipofectamine RNAiMAX (Invitrogen) according to the manufacturer's instructions. The efficiency of transfection was tested by using qPCR with a more than 50% transduction rate.

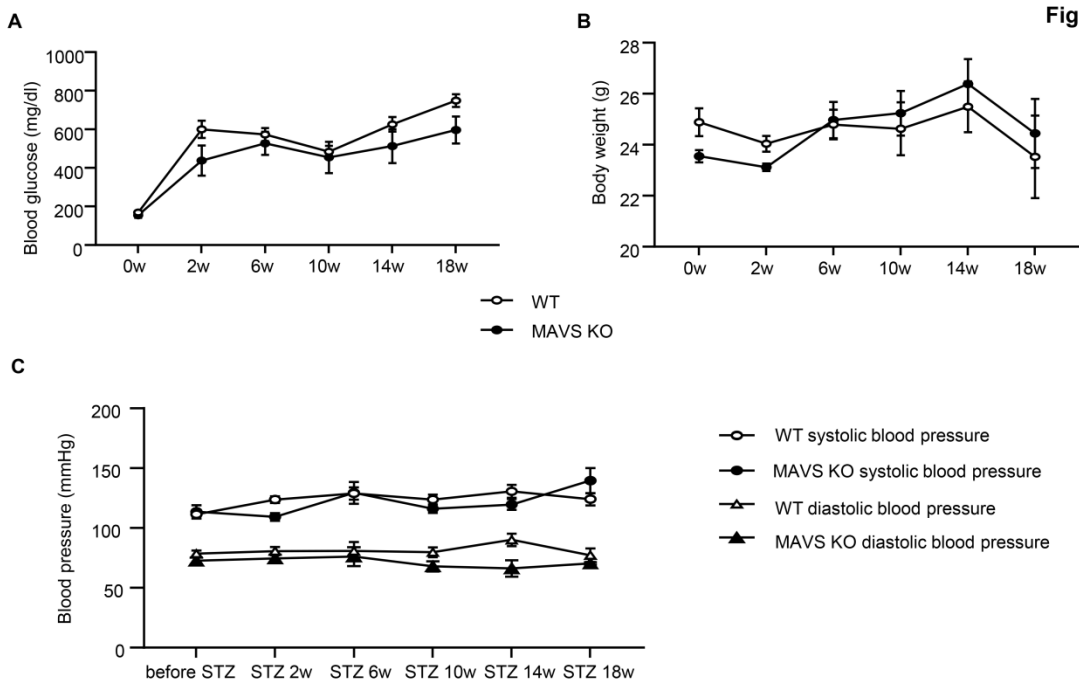
For high glucose stimulation, cultured cells were stimulated with the cultured medium containing 25 mM D-glucose (FUJIFILM) (high glucose - HG) or 25 mM L-glucose (Sigma Aldrich) (osmotic control - OSM) at the indicated time. For *K. oxytoca* stimulation, human

IECs were challenged with live bacteria. For IL-6 or IL-17 induction, cultured cells were stimulated with recombinant human/murine IL-6 or IL-17 (R&D) at the indicated concentration and time.

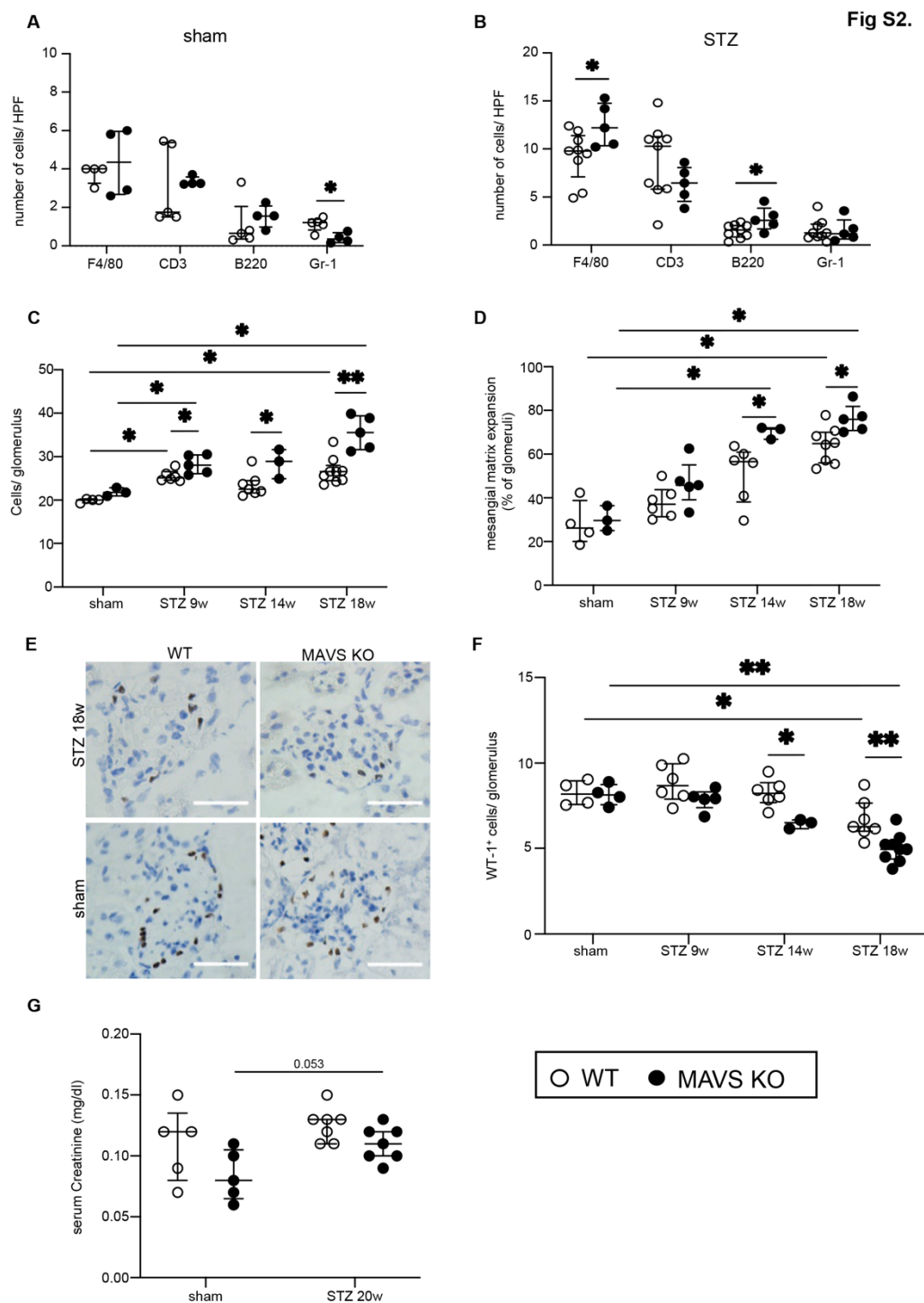
Assessment of podocyte cell death

After indicated time for cell treatment, cells were harvested and resuspended 1×10^5 cells in 200 μL of Annexin V binding buffer (10 mM HEPES, 150 mM NaCl, 2.5 mM CaCl₂ in PBS (pH 7.4)), containing 1 μL of Annexin V-FITC (Medical & Biological Laboratories) and 1 μL of PI (Immunostep Biotech) incubate in 15 min then run on a BD FACS Calibur cytometer. PI⁻Annexin V⁺ cells = apoptotic cells. PI⁺ Annexin V⁺ cells = necrotic cells.

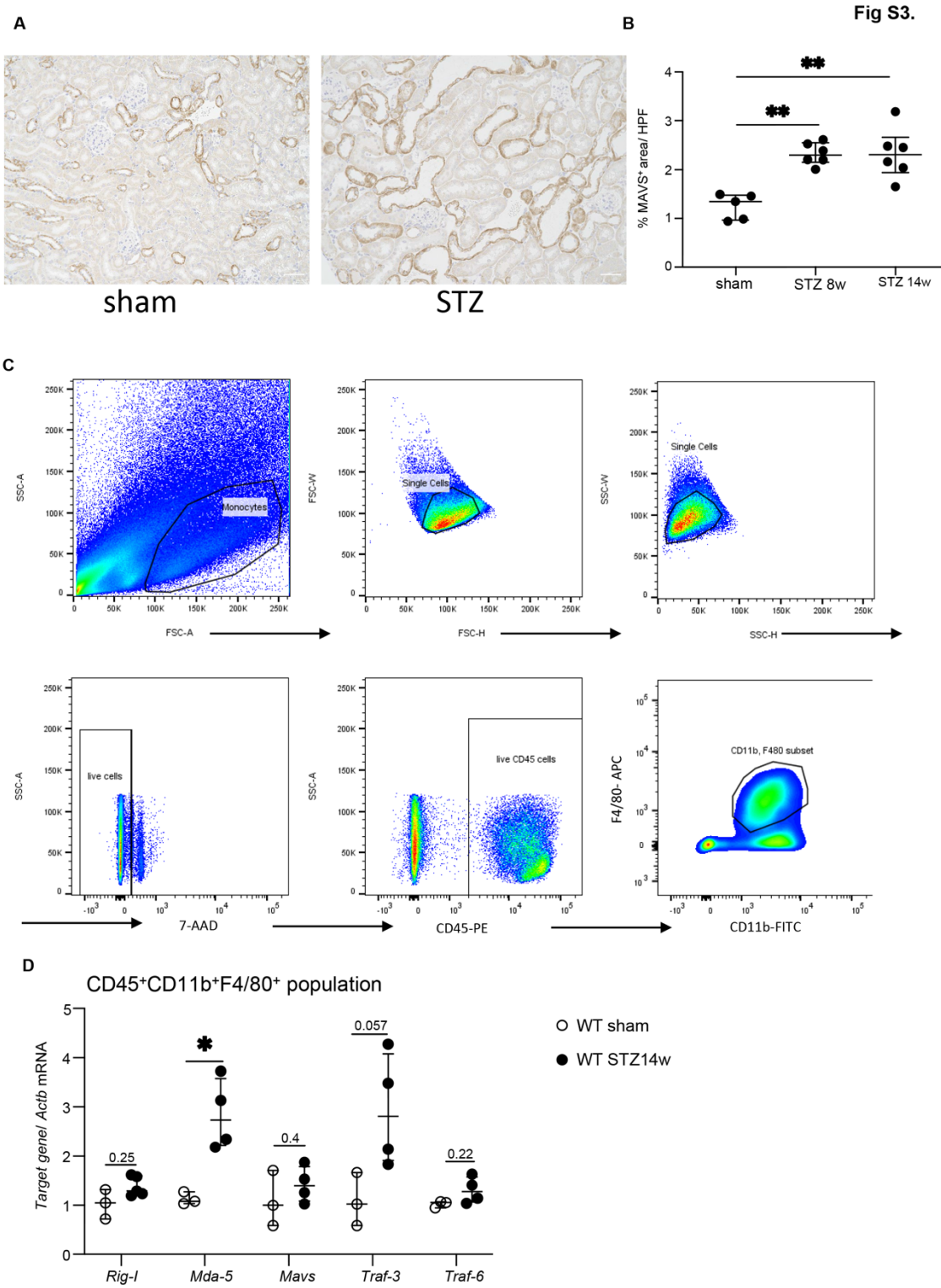
Fig S1.



Supplemental Figure 1. WT and MAVS KO mice developed equivalent degrees of hyperglycemia. Blood glucose (A), body weight (B) and blood pressure (C) were shown. Data are shown as median \pm IQR; * $p < 0.05$; ** $p < 0.01$

Fig S2.

Supplemental Figure 2. Mitochondrial antiviral signaling protein (MAVS) deficiency promotes glomerular injury in diabetic conditions. F4/80, CD3, B220, and Gr-1 cells were examined by immunohistochemistry staining in sham and diabetic mice (A, B). Glomerular hypercellularity (C), and mesangial expansion (D). The loss of podocytes is assessed by Wilms tumor 1 (WT-1) staining (1000 X, scale bar = 50 μ m) (E, F). Serum creatinine levels (G). Data are shown as median \pm IQR; * p < 0.05; ** p < 0.01

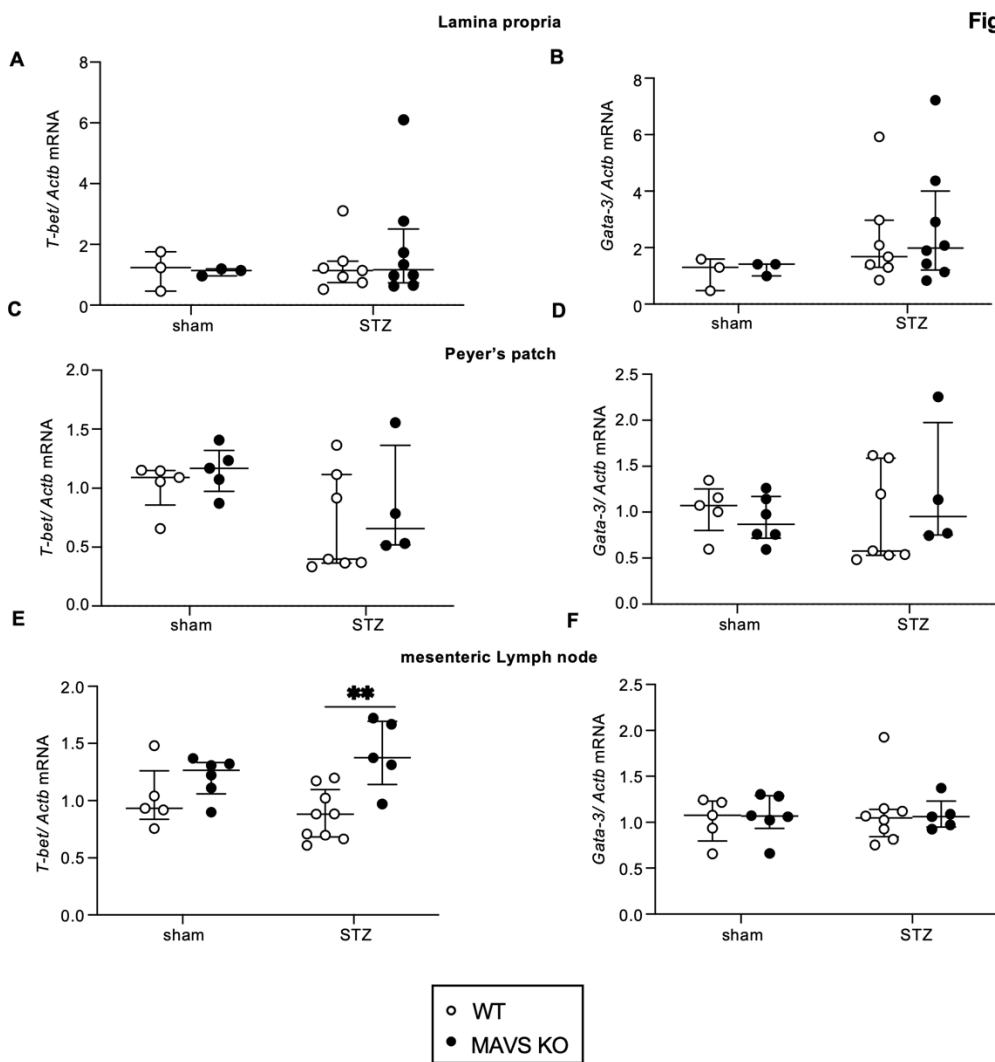
Fig S3.

Supplemental Figure 3. MAVS expression in the kidney and macrophages of WT diabetic mice. MAVS expression in the kidney of WT sham and WT diabetic mice (A, B). FACS sorting strategy for renal macrophages (C). *Rig-I*, *Mda-5*, *Mavs*, *Traf-3*, *Traf-6* mRNA expression in kidney-isolated macrophages from WT sham and diabetic mice (D). Data are shown as median \pm IQR; * $p < 0.05$; ** $p < 0.01$

Fig S4.

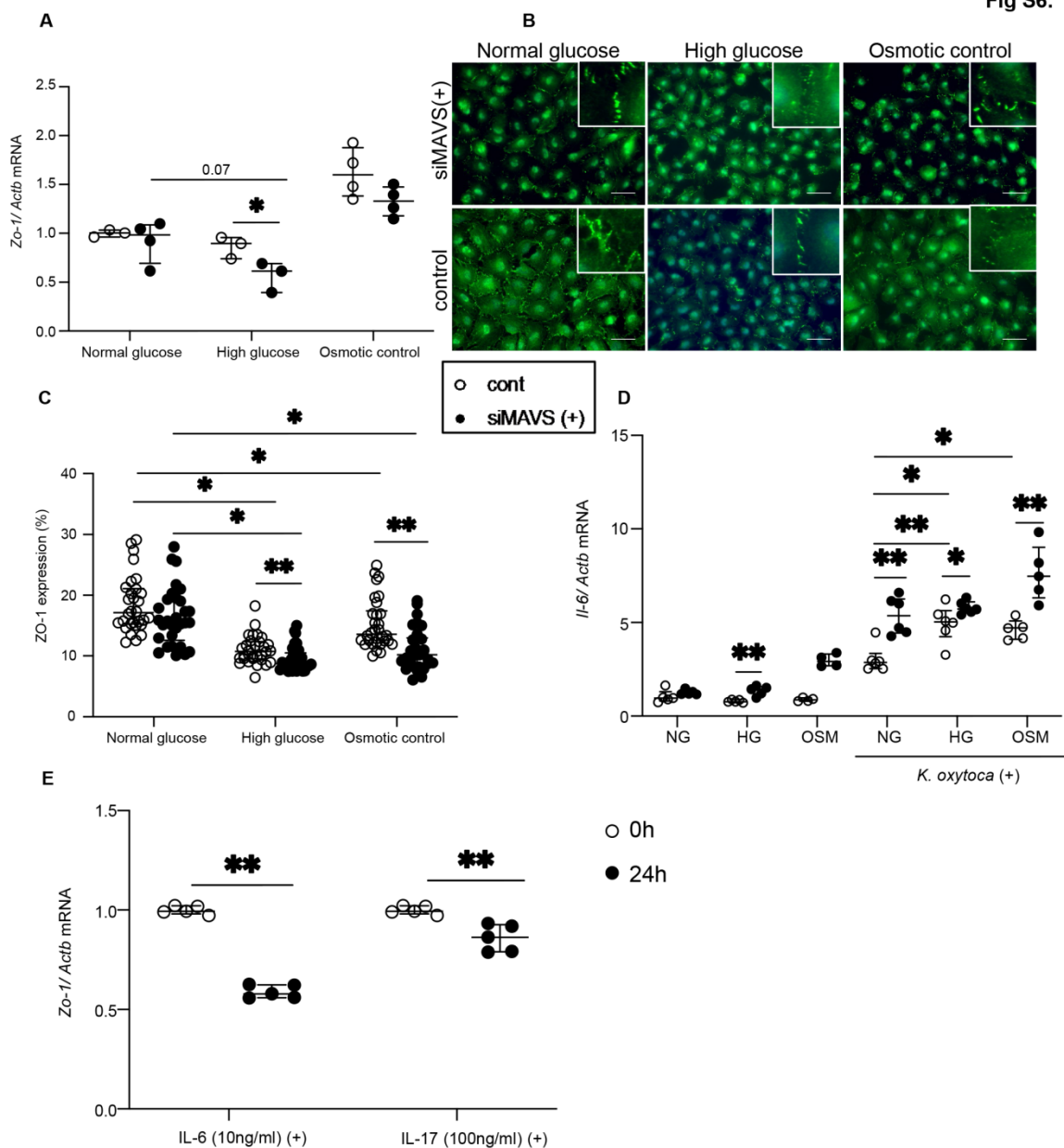
	Spleen				Mesenteric lymph nodes			
	WT	MAVS KO	WT + STZ	MAVS KO + STZ	WT	MAVS KO	WT + STZ	MAVS KO + STZ
<i>Klebsiella oxytoca</i>								
<i>Enterococcus faecalis</i>								
<i>Escherichia coli</i>								
<i>Providencia rettgeri</i>								
<i>Proteus mirabilis</i>								
<i>Klebsiella pneumonia</i>								
<i>Myroides odoramimius</i>								
<i>Aerococcus viridans</i>								
<i>Lactococcus lactis</i>								
<i>Vagococcus fluvialis</i>								

Supplemental Figure 4. Bacterial strains in the spleen and mesenteric lymph node culture

Fig S5.

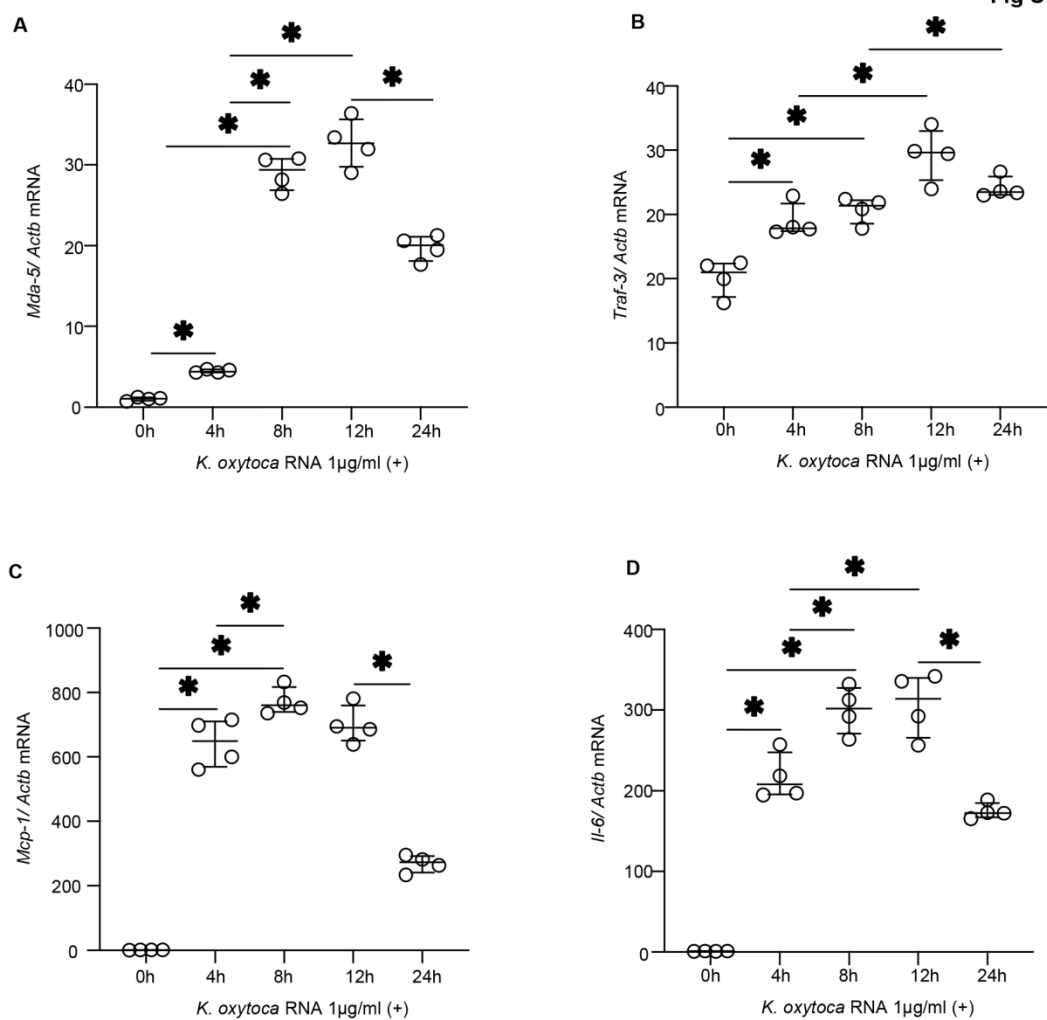
Supplemental Figure 5. An intestinal inflammatory condition in the control and diabetic mice. The expression of the transcription factor *T-bet* and *Gata-3* in lamina propria (A, B), Peyer's patch (C, D), and mesenteric lymph node (E, F) of WT and MAVS KO sham or diabetic mice. Data are shown as median \pm IQR; * p < 0.05; ** p < 0.01

Fig S6.



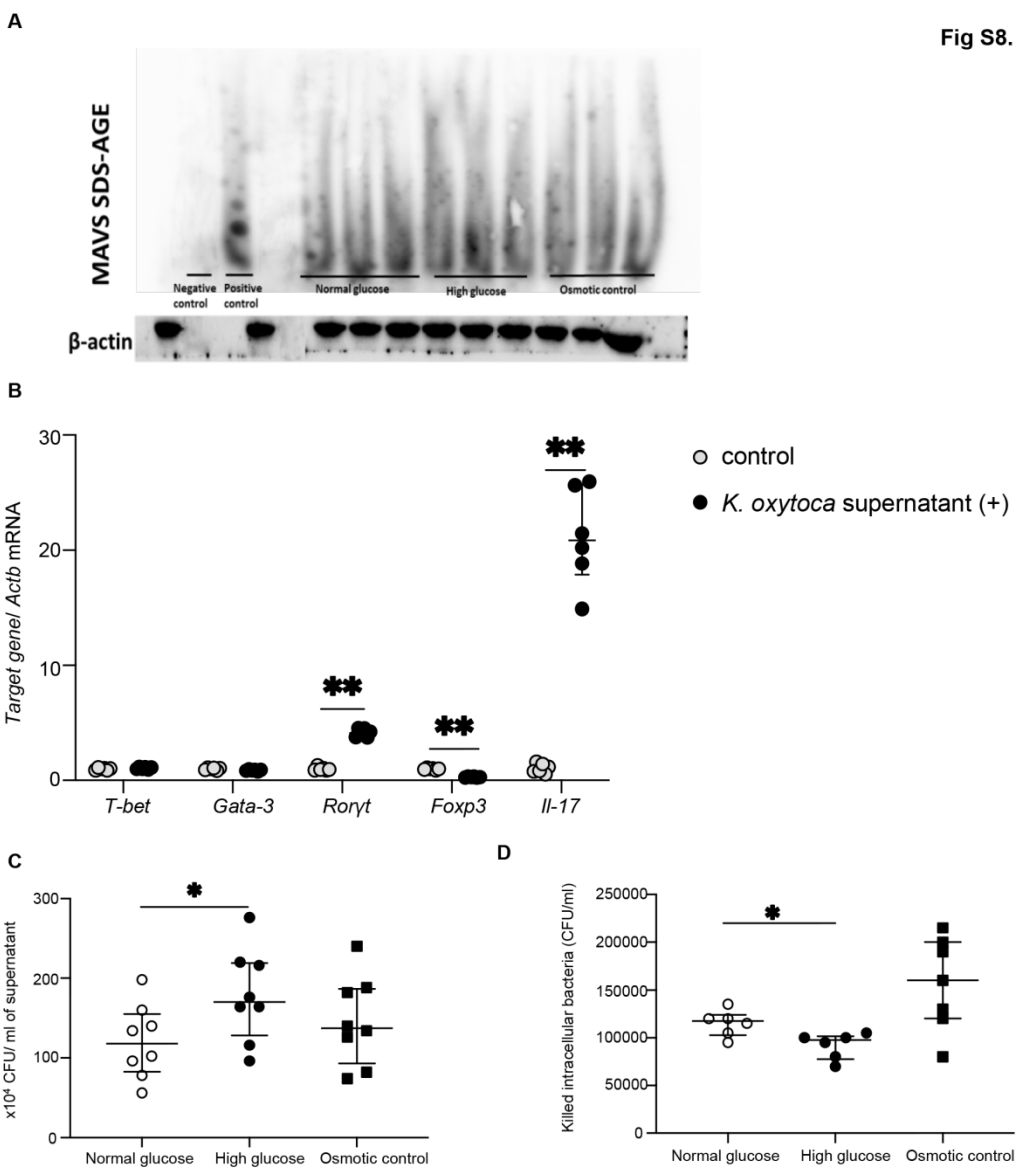
Supplemental Figure 6. Experiments with human intestinal epithelial cells. Zonula occludens (*Zo-1*) mRNA expression (24 h stimulation) (A) and ZO-1 staining (48 h stimulation) (B, C) under normal glucose (NG), high glucose (HG), and osmotic control (OSM) conditions. mRNA expression of *Il-6* (D) under NG, HG, and OSM conditions with and without coculture with *Klebsiella oxytoca* for 4 h. *Zo-1* expression 24h after IL-6 or IL-17 stimulation (E). Data are shown as median \pm IQR; * $p < 0.05$; ** $p < 0.01$

Fig S7.

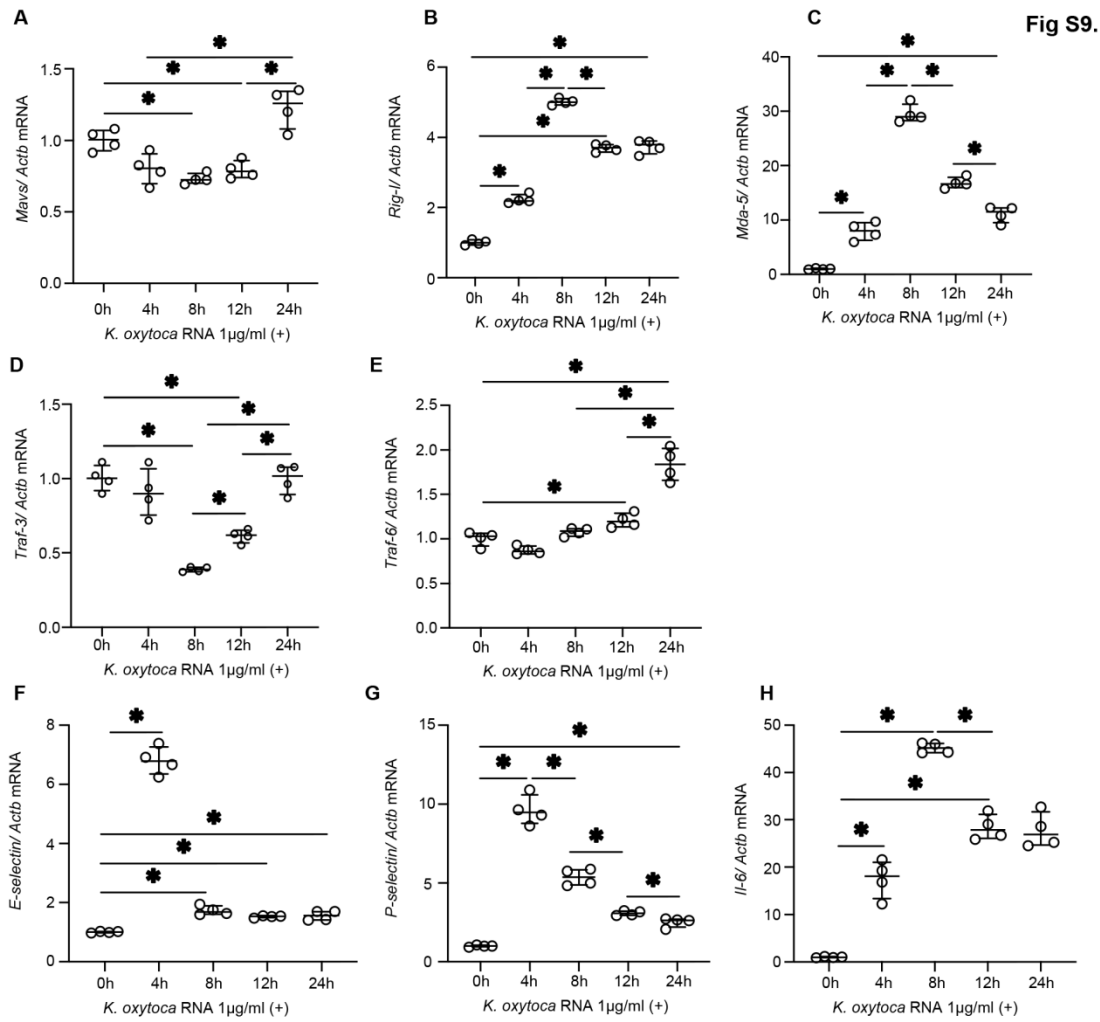


Supplemental Figure 7. *K. oxytoca* activates RIG-I/MDA-5–MAVS–TRAF-3/TRAF-6 signaling pathway in TECs. *Mda-5* (A), *Traf-3* (B), *Mcp-1* (C), *Il-6* (D) mRNA were shown under *K. oxytoca* RNA transfection. Data are shown as median \pm IQR; * $p < 0.05$; ** $p < 0.01$

Fig S8.

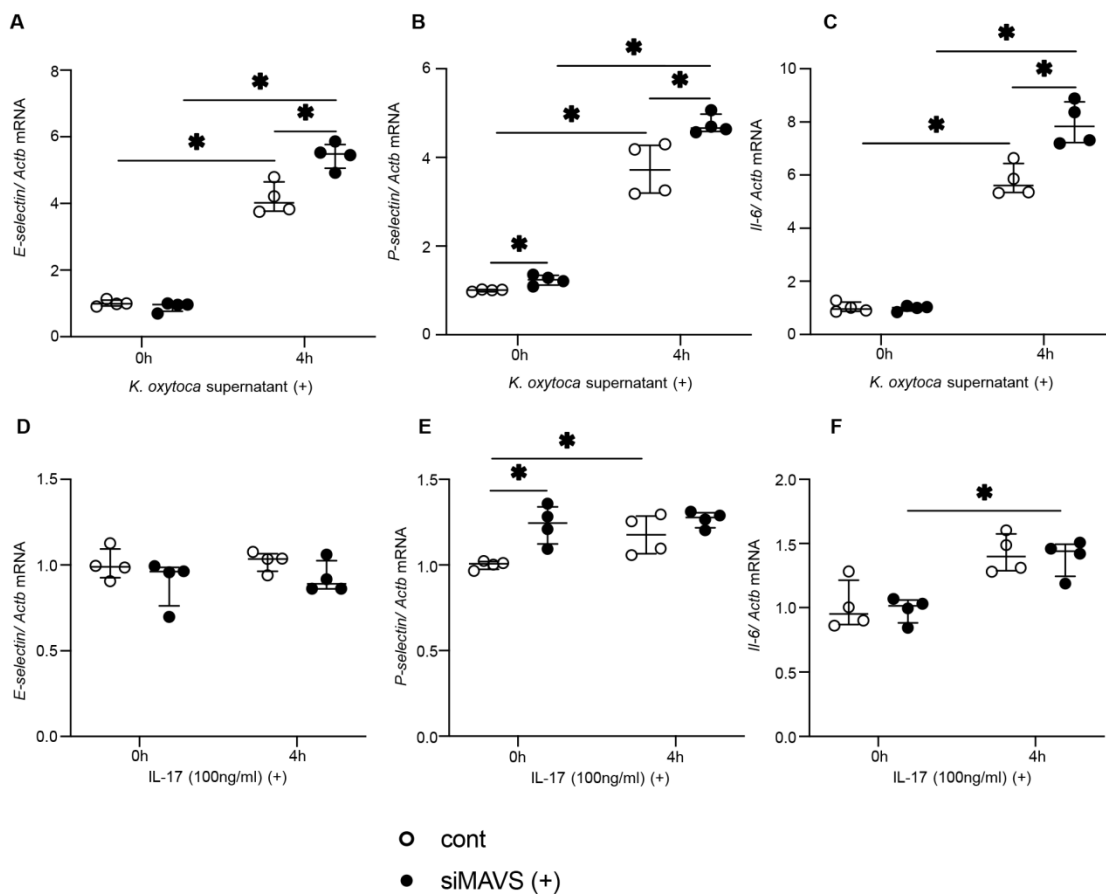


Supplemental Figure 8. The dysfunction of bone marrow-derived macrophages (BMDMs). Detect MAVS aggregation by SDS-AGE after high glucose stimulation for 8 h in BMDMs (A). *T-bet*, *Gata-3*, *Ror γ t*, *Foxp3*, *Il-17* mRNA expression in T cells at 72 h after coculture with *K. oxytoca* supernatant- activated or control BMDMs (B). Phagocytic activity (C) and intracellular bacterial killing activity (D) to *K. oxytoca* of long-term NG, HG, or OSM-exposed BMDMs. Data are shown as median \pm IQR; * p < 0.05; ** p < 0.01



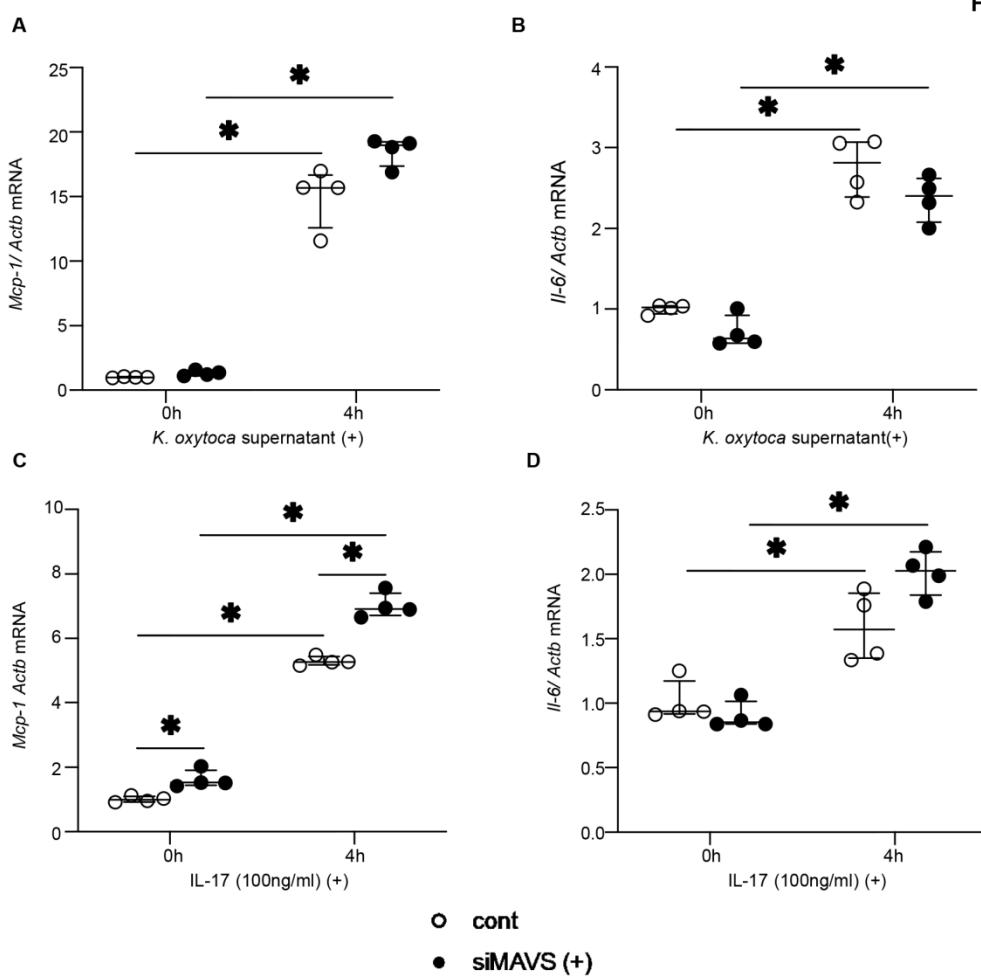
Supplemental Figure 9. *K. oxytoca* supernatant activates RIG-I/MDA-5-MAVS-TRAF-3/TRAFF-6 signaling pathway in glomerular endothelial cells (GECs). *Mavs* (A), *Mda-5* (B), *Rig-I* (C), *Traf-3* (D), *Traf-6* (E) mRNA were upregulated under *K. oxytoca* RNA transfection. Activated markers *E-selectin* (F), *P-selectin* (G), *Il-6* (H) were shown. Data are shown as median \pm IQR; * p< 0.05; ** p< 0.01

Fig S10.



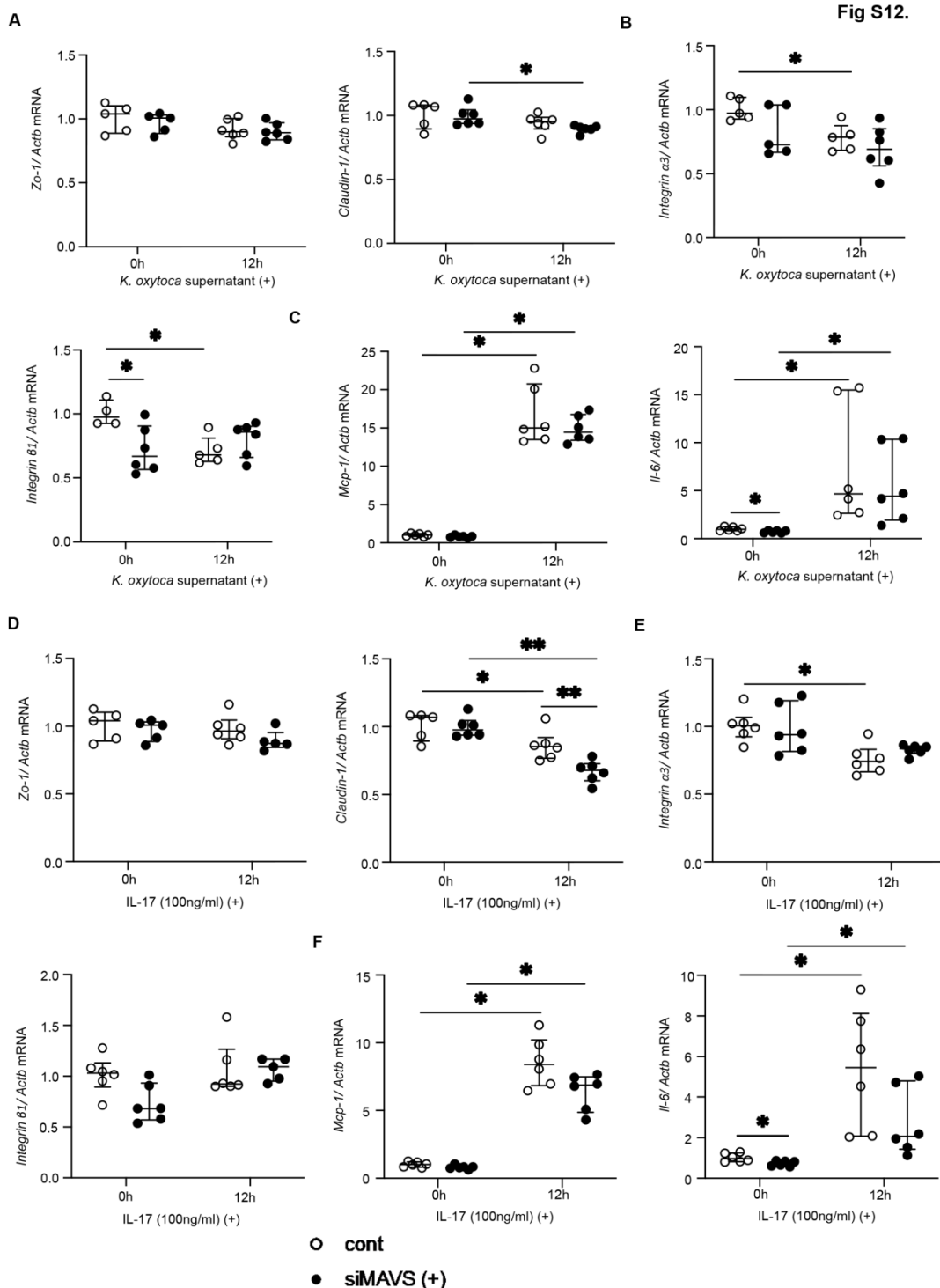
Supplemental Figure 10. The effect of *K. oxytoca* supernatant and IL-17 on glomerular endothelial cells (GECs) under normal and MAVS knockdown conditions. Levels of *E-selectin*, *P-selectin*, *Il-6* mRNA after 4h *K. oxytoca* supernatant stimulation (1:20) (A–C) or IL-17 stimulation (100ng/ml) (D–F). Data are shown as median \pm IQR; * $p<0.05$; ** $p<0.01$

Fig S11.



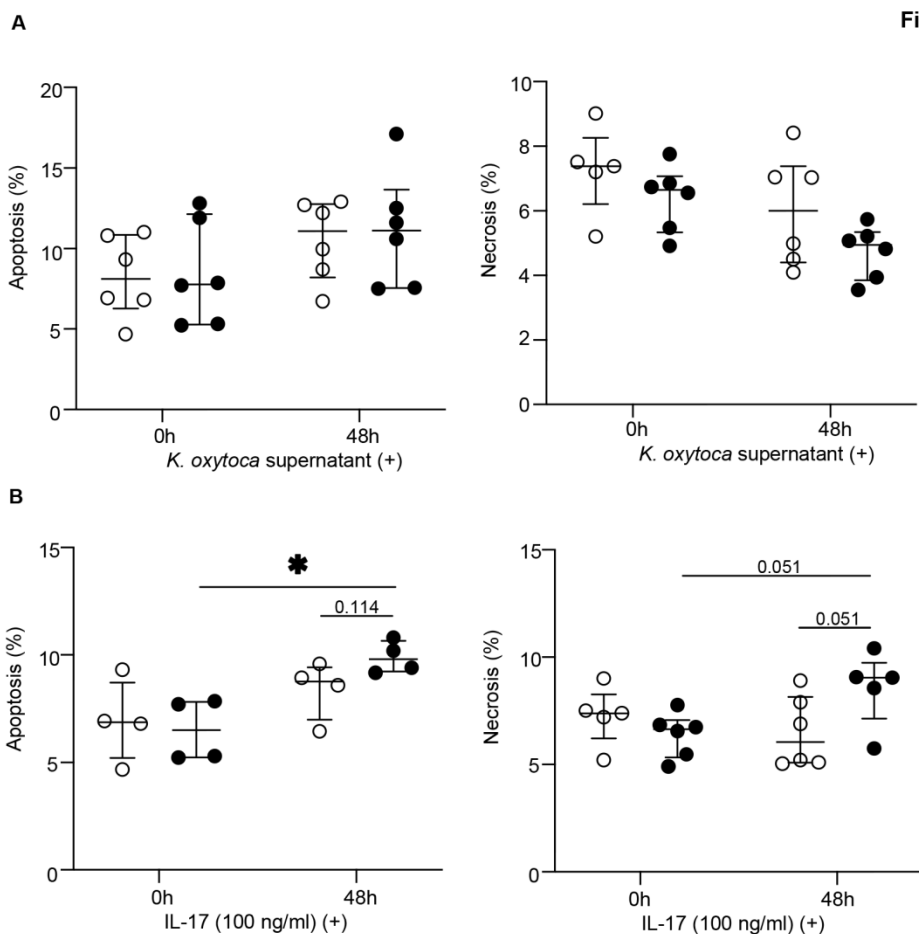
Supplemental Figure 11. The effect of *K. oxytoca* supernatant and IL-17 on mesangial cells under normal and MAVS knockdown conditions. Levels of pro-inflammatory cytokines *Mcp-1*, *Il-6* after 4 h of *K. oxytoca* supernatant stimulation (1:20) (A, B) or IL-17 stimulation (100ng/ml) (C, D). Data are shown as median \pm IQR; * $p<0.05$; ** $p<0.01$

Fig S12.



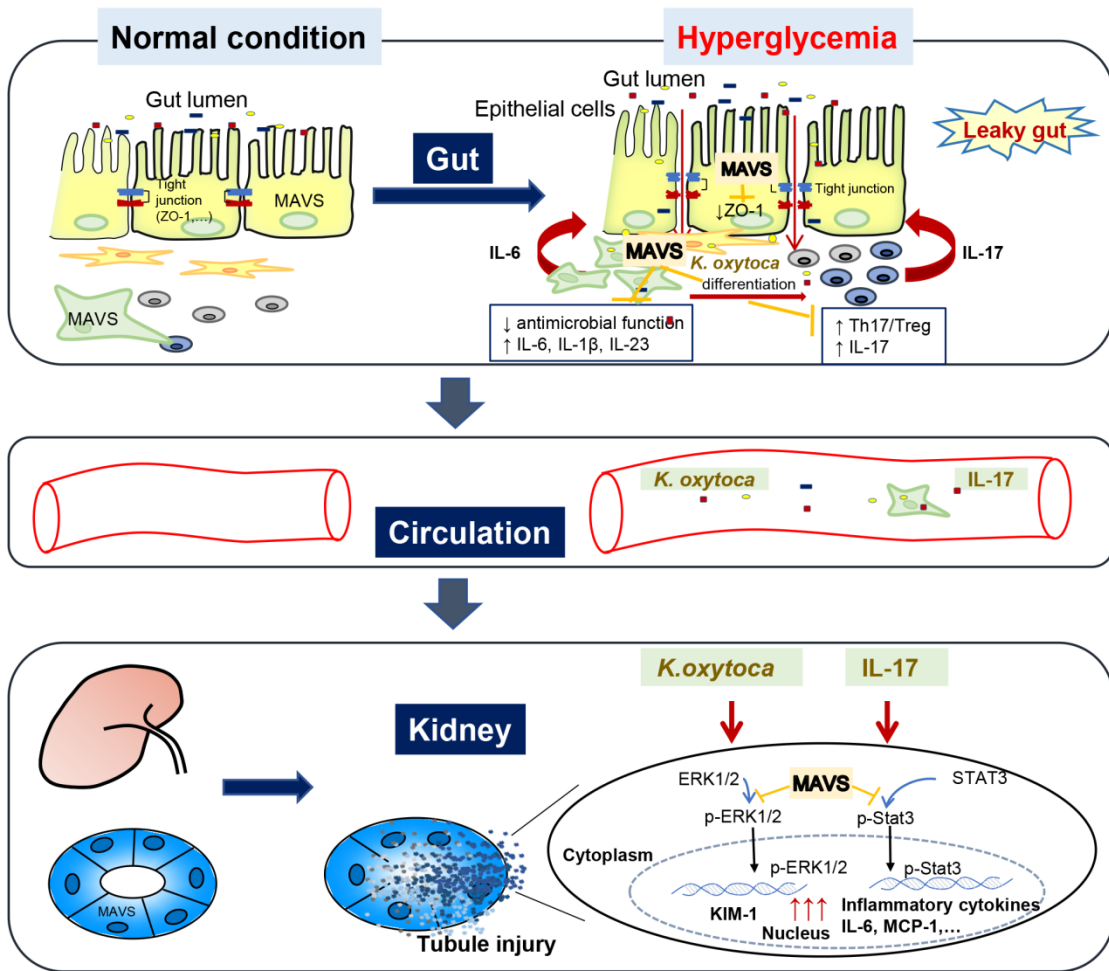
Supplemental Figure 12. The effect of *K. oxytoca* and IL-17 on immortalized conditional culture podocytes. *Tight junction* (*Zo-1*, *claudin-1*) (A), *integrin* ($\alpha 3$, $\beta 1$) (B), *proinflammatory cytokines* (*Mcp-1*, *Il-6*) (C) mRNA expression after *K. oxytoca* supernatant stimulation (1:20) with and without siMAVS. *Tight junction* (*Zo-1*, *claudin-1*) (D), *integrin* ($\alpha 3$, $\beta 1$) (E), *proinflammatory cytokines* (*Mcp-1*, *Il-6*) (F) mRNA expression after IL-17 treatment (100ng/ml) with and without siMAVS. Data are shown as median \pm IQR; * $p < 0.05$; ** $p < 0.01$

Fig S13.



Supplemental Figure 13. The effect of *K. oxytoca* and IL-17 to cell death on immortalized conditional culture podocytes. Apoptotic and necrotic cells were measured after *K. oxytoca* supernatant (1:20) treatment (A) or IL17 treatment (B). Data are shown as median \pm IQR; * $p<0.05$; ** $p<0.01$

Fig S14.



Supplemental Figure 14. Schematic graphic: Chronic hyperglycemia leads to a “leaky gut” and an inflammatory intestine with notably IL-17 up-regulation to promote the translocation of bacteria, including *K. oxytoca* and IL-17 to extraintestinal sites and blood circulation. Then, bacteremia and IL-17 turn back to worsen gut dysfunction and accelerate kidney injury. Systemic MAVS is reno-protective in DKD mice by an intestinal protective role and the dominant inhibitory effects on suppressing KIM-1 production under *K. oxytoca* supernatant or IL-17 stimulation.

Supplemental Table 1 List of primers used for RT-qPCR

Mouse		Forward	Reverse
	<i>Mcp-1</i>	CTTCCTCCACCACCATGCA	CCAGCCGGCAACTGTGA
	<i>Il-17</i>	CTCCAGAAGGCCCTCAGACTAC	AGCTTCCCTCCGCATTGACACAG
	<i>Il-6</i>	TGGCTAAGGACCAAGACCATCAA	AACGCACTAGGTTGCCGAGTAGA
	<i>Tnf-α</i>	ATCCGCGACGTGGAACGT	ACCGCCTGGACTTCTGGAA
	<i>Il-23p19</i>	TGCTGGATTGCAGAGCAGTAA	ATGCAGAGATTCCGAGAGA
	<i>Zo-1</i>	AGCTCATAGTTAACACAGCCTCCAG	TTCTCCACAGCTGAAGGACTCACAG
	<i>Kim-1</i>	CTATGTTGGCATCTGCATCG	AAGGCAACCACGCTTAGAGA
	<i>Roryt</i>	CAGCAGCAACAGGAACAAGTG	CCCATCTGAGAGGCCCTAAAGTG
	<i>Foxp3</i>	GGCGAAAGTGGCAGAGAGG	AAGGCAGAGTCAGGAGAAGTTG
	<i>Tgβ</i>	GAGCGCTCATCTGATTTTA	TGAGGCTCTGACACCAAGGT
	<i>Il-1β</i>	GGATGAGGACATGAGCACCT	AGCTCATATGGGTCCGACAG
	<i>Mavs</i>	GCGAGGTCCACTGAGCTATC	CAGGTCAAGGAGCAATGGAGG
	<i>Rig-I</i>	GCGGCGCCGAATAGTTT	GTTAACCCCTCCCCACCAT
	<i>Mda-5</i>	GTGATGACGAGGCCAGCAGTTG	ATTCATCCGTTCTGCCAGTTCA
	<i>Traf-3</i>	GCCC GT CCT CC CTT TAGTG	GGCCACCTCGCATAGGAA
	<i>Traf-6</i>	CCCAGTTGCACATGAGACTGTT	CGGACGCAAAGCAAGGTTAA
	<i>Claudin-1</i>	CTGGAAGATGATGAGGTGCAGAAGA	CCACTAATGTCGCCAGACCTGAA
	<i>Integrinα3</i>	AGCAACCTGCAGATGCGAGC	CTCATGCGCATCTCCCCAG
	<i>Integrinβ1</i>	TTTGCAACACCAAGCTCAC	TTTCCAACCTGCATGTGAA
	<i>E-selectin</i>	AGCTACCCATGGAACACGAC	ACGCAAGTTCTCCAGCTGTT
	<i>P-selectin</i>	GTCCACGGAGAGTTGGTGT	AAGTGGTGTTCGGACCAAAG
	<i>β-actin</i>	AGCCATGTACGTAGCCATCC	CTCTCAGCTGTGGTGGTCAAAG
human	<i>Zo-1</i>	TGCCATTACACGGCTCTG	GTTGATGATGCTGGTTGTT
	<i>Il-6</i>	TGCAGAAAAGGCAAAGAATCTAG	CGTCAGCAGGCTGGCATT
	<i>β-actin</i>	AGGCACCAGGGCGTGAT	GCCCCACATAGGAATCCTCTGAC